Flux Jump Analysis on Superconducting Nb_3Sn Accelerator Magnets

Conor Donnelly
University of Pennsylvania

Supervisor: Giorgio Ambrosio - Fermilab

Associate Supervisor: Guram Chlachidze - Fermilab

Contents

Table of Figures

1. Abstract

The upper limit of performance of the current superconducting magnet technology, NbTi, will have been reached with the operation of the Large Hadron Collider (LHC) at CERN in Geneva, Switzerland in 2008. A new magnet technology, Nb_3Sn, promises greater critical current density and applied field thresholds; however, thermo-magnetic instabilities, or flux jumps, are inevitable with this magnet technology and have yet to be analyzed in depth. Understanding these thermal instabilities will lead to greater magnetic stability for future high field accelerator magnets. Using a new automated spike analysis program along with the existing method, it was found that a current dependent spike magnitude threshold could aid in protecting the integrity of the magnet from premature quenching. This work reports preliminary analysis of flux jumps in superconducting Nb_3Sn magnets.

2. Introduction

2.1 Introduction to Fermilab

Fermi National Accelerator Laboratory in Batavia, Illinois is home to the world's highest energy particle accelerator. Using the aptly named Tevatron, protons and anti-protons are accelerated to about 99.99997 percent of the speed of light and then collided at two places in the Tevatron ring, the Collision Detector at Fermilab (CDF) and DZero (DØ). At these points, 5000 ton detectors observe the results of the high energy collisions. Magnets are used to accelerate, bend, and focus the particles; however, accelerating the particles using a conventional electromagnet would generate an enormous amount of heat, which would pose a major problem for the functionality of the magnet. Therefore, Fermilab uses superconducting magnets to bend and focus the protons and anti-protons in the Tevatron. The main draw of these magnets is with their essentially zero resistance current can run though the coils of the magnet with little energy loss due to electrical resistance. An elaborate cryogenic system is needed to keep the magnets cold, as they are operated below 5 K to achieve maximum results.

2.2 Introduction to Superconductivity

Fermilab currently uses superconducting NbTi magnets to bend and focus particles in the Tevatron. The idea of superconductivity was first established about a century ago; a background to superconductivity will now be presented.

2.2.1 History of Superconductivity

Superconductivity was discovered by Kamerlingh Onnes in 1911 while testing the temperature dependence of the resistance of Mercury; he found that at a specific temperature, the resistance of the material became essentially zero. This temperature, now called the critical temperature of a superconductor (T_c), is the temperature at which a material changes from a normal resistive state to a superconducting state. This is illustrated in Figure 1 [1].

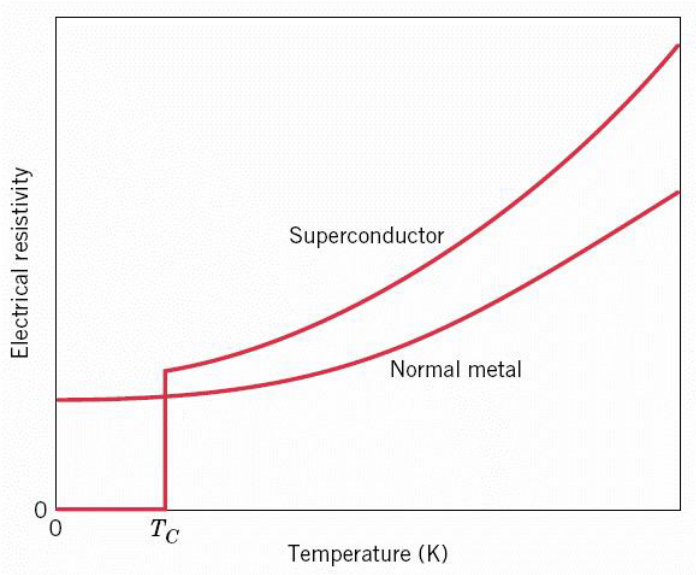

Figure 1: Temperature Dependence of Resistivity for Metals and Superconductors

The next major discovery in the area of superconductivity was made by Walther Meissner and Robert Ochsenfeld in 1933. They found that when a superconductor is

below its critical temperature, it excludes weak magnetic fields from its bulk; this is called the Meissner Effect and is shown in Figure 2 [1].

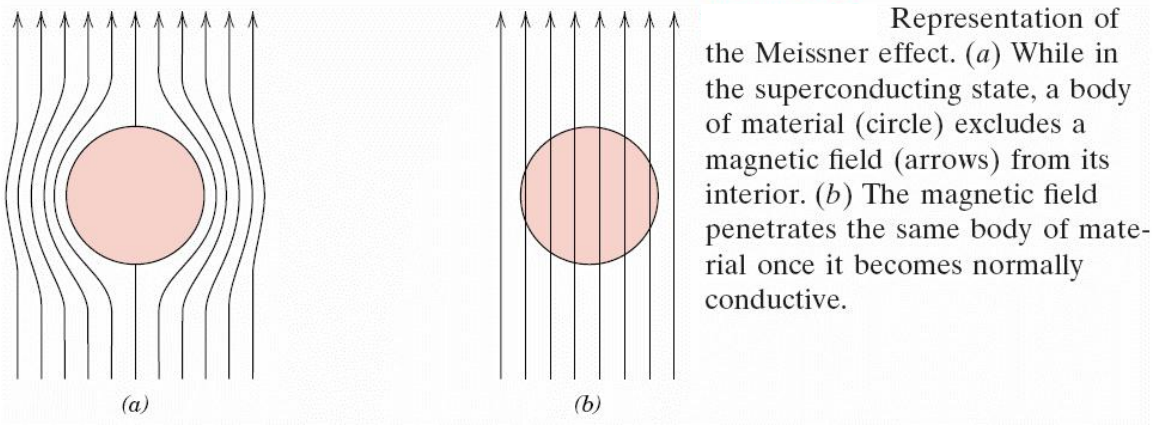

Representation of the Meissner effect. (*a*) While in the superconducting state, a body of material (circle) excludes a magnetic field (arrows) from its interior. (*b*) The magnetic field penetrates the same body of material once it becomes normally conductive.

Figure 2: Field Exclusion in a Superconductor

An interesting application of this effect is the idea of magnetic levitation. When an external magnetic field is applied to a conductor, a current is produced in the conductor to oppose the change in magnetic flux (Lenz's Law). In a perfect conductor (a perfect diamagnet), the current would meet no resistance, as it would persist in any magnitude necessary to completely cancel out the change in external flux. A superconductor is a perfect diamagnet with one main difference: A superconductor excludes any magnetic field from its bulk as the phase change to the superconducting state takes place. Therefore, when a magnet is placed near a superconductor, induced super currents will produce mirror images of the poles of the magnet, creating a repulsive force. When the force of gravity equals the force with which the superconductor is "pushing," levitation occurs, as shown in Figure 3 [2].

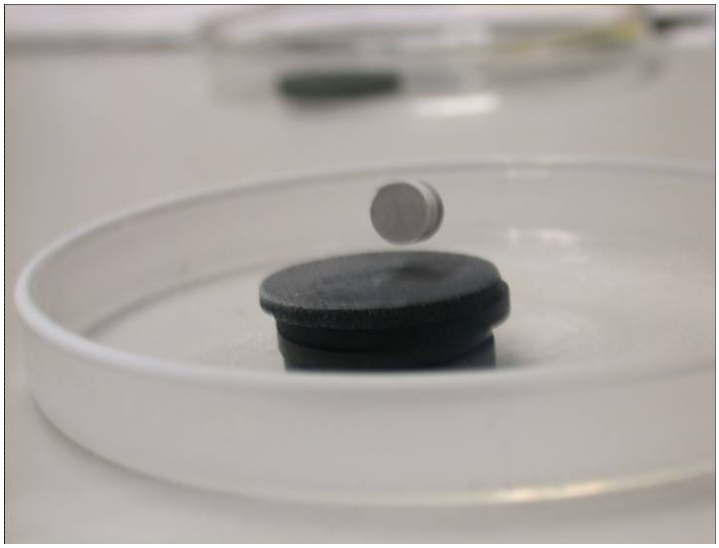

Figure 3: Magnetic Levitation due to Meissner Effect

In the middle of the 20th Century, another type of superconductivity was found for metallic alloys that did not exist for pure elements. Materials that show this second class of superconductivity, called Type II superconductivity, have a phase where they do not completely expel applied fields from their body. Rather, discrete lines of flux, called fluxons or vortex lines, penetrate the superconductor. The material is only superconducting when the fluxons are stationary, or "pinned;" if these fluxons move, the superconductor becomes resistive.

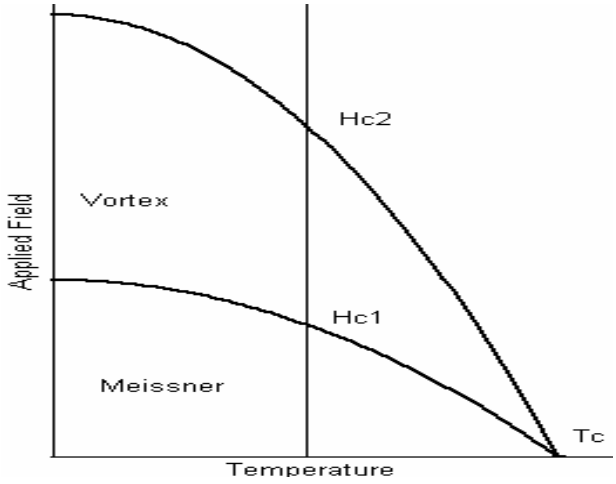

Figure 4: Phase Diagram for Type II Superconductors

When the applied field is below H_{c1} in figure 4, the Meissner Effect dominates and the applied field is completely expelled from the body of the superconductor. When the applied field is between H_{c1} and H_{c2}, vortex lines are allowed to pass through the superconductor (Figure 5). Above H_{c2}, the material goes back to its normal resistive state. In particle accelerators, only Type II superconductors are used because of the need for high applied magnetic fields.

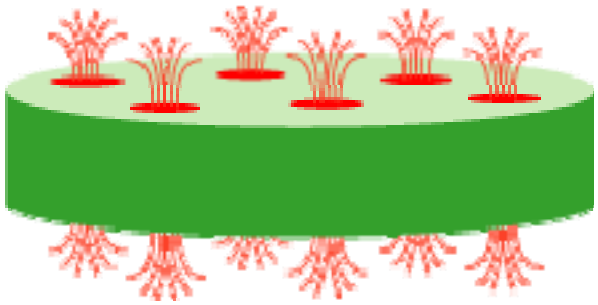

Figure 5: Vortex Lines in a Type II Superconductor

The most recent important development in superconductivity occurred in the 1980's when J. Georg Bednorz and K. Alexander Müller discovered ceramic Copper Oxides that became superconducting at temperatures above that of liquid Nitrogen (77 K). They were awarded the Nobel Prize for their work [4].

Thus far, two limiting factors for the superconducting state have been discussed, applied field and temperature. However, a third parameter does exist: current density. The combination of these three parameters leads to the idea of a critical surface (Figure 6), which is the boundary between the superconducting state and the normal resistive state.

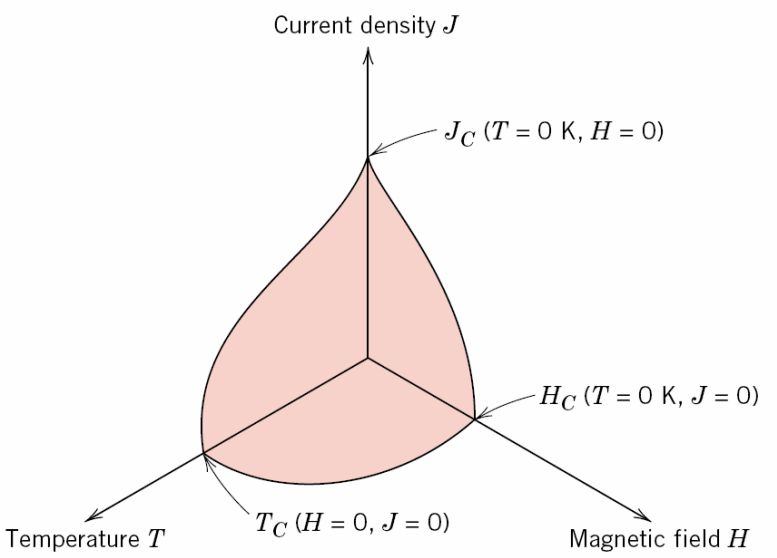

Figure 6: Critical Surface of a Superconductor

At all points inside of this surface, the material is superconducting; at all points outside this surface, the material acts as a normal conductor.

2.2.2 Flux Jumps

When superconducting magnets are used in particle accelerators, the highest particle energy possible is desired; however, in order to do this, the magnet must be used at a point very close to the boundary of the critical surface of that material. When a high, but below the critical current density, current is run through a superconductor, a force is exerted on the fluxons within the superconductor. If these forces are great enough, the fluxons could potentially shift, causing the material to become locally resistive; this is called a flux jump. The severity of the flux jump determines what happens next. Because $P = I^2R$ and I is in the thousands of Amps and R is large as well (due to the fact that most superconductors are poor normal conductors), a huge amount of heat could be generated when these fluxons move. If the heat generated is convergent, the heat will dissipate throughout the magnet and the material will return to a superconducting state. However, if the material is unable to recover from the amount of heat generated, the magnet "quenches," which means it goes through an irreversible transition to the normal resistive state. In order to protect the superconducting material, it is usually placed in a

Copper matrix so that the Copper, a good electrical conductor (and thermal conductor, due to the Weidemann-Franz Law) will dissipate both the current and heat when a flux jump occurs. Without this Copper matrix, the material would have little chance of recovering its superconducting state [6].

2.3 Superconducting Nb_3Sn Magnet Research at Fermilab

With the background of superconductivity in place, the work of the Measurement and Analysis Group in the Magnetic Systems Department in the Technical Division at Fermilab can now be explained.

2.3.1 Advantages of Nb_3Sn

Currently in the Tevatron, a Niobium Titanium (NbTi) alloy is being used to accelerate the protons and anti-protons. However, the technological limit of the NbTi will have been reached when the Large Hadron Collider at CERN becomes operational within the next year. Therefore, a new material is needed to replace the current NbTi technology; it has been decided that the best candidate is Nb_3Sn because it offers a higher maximum applied field as well as critical current density than NbTi at constant temperature (Figure 7, adapted from [5]).

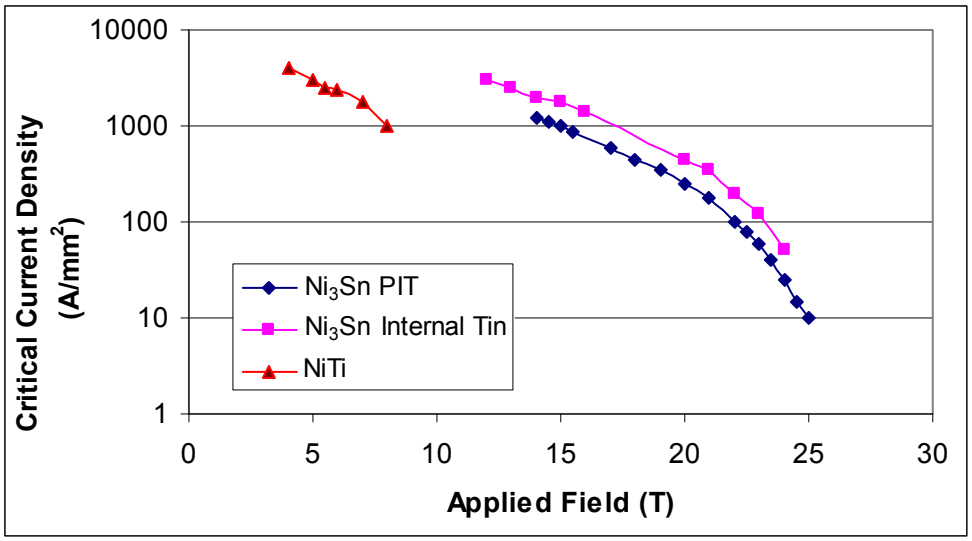

Figure 7: Critical Current Density versus Applied Field for Nb_3Sn

The two different Nb_3Sn lines in Figure 7 are simply different processing techniques to process the superconductor, which is to be discussed later in this paper. As shown, Nb_3Sn achieves the same, if not greater, critical current threshold as NbTi but at an applied field an order of magnitude greater.

2.3.2 Disadvantages of Nb_3Sn

There are two drawbacks of Nb_3Sn. The first is that Nb_3Sn is a very brittle (easily fractured) material, which is mainly due to the fact that Nb_3Sn is an intermetallic compound. This is in direct contrast to NbTi, which is a ductile alloy of Niobium and Titanium. Although these terms are often used synonymously, there is a subtle difference between an alloy and an intermetallic compound; to examine this, we will look at the crystal structure of both materials.

2.3.2.1 A Material Science Perspective

When looking at a material microscopically, it is convention to look at the unit cell of the material, which is the way the atoms are arranged in the smallest repeating unit. Superconducting NbTi is a body centered cubic (BCC), solid solution alloy that has a roughly 1:1 Niobium to Titanium ratio throughout its crystal structure. A body centered cubic arrangement means that there is one atom on each corner of the cube (8 total) and one atom in the center of the cube. Taking into account that each atom on the corners of the cube is shared by 8 other cells and that the atom in the center is unique to each unit cell, there are 2 equivalent atoms per unit cell. For NbTi, homogeneity predicts that one of the equivalent atoms is Niobium and the other Titanium. The BCC structure for this alloy, where the blue atoms are either Niobium or Titanium, controlled only by the need for an approximate 1:1 ratio, is shown in Figure 8.

Figure 8: BCC Structure of NbTi

This crystal structure leads to a ductile material that can be easily drawn into wires for magnet fabrication.

Nb_3Sn has a similar, but noticeably different structure called A-15 crystal structure. This structure is similar in that there is a BCC core to the A-15 structure; the difference is the atoms at the corners and at the center of the crystal are all Tin atoms. The Niobium atoms lie on the face of each side of the cube, two per face. Doing the same analysis as with NbTi, that is 2 equivalent Tin atoms (one at each corner of the cube divided by 8 because it is shared among 8 other unit cells plus the one atom in the center) and 6 Niobium atoms (two per face of the cube divided by 2 because each of those atoms is shared by two unit cells). This structure, which gives the correct Niobium to Tin ratio but

also leads to a very brittle material, is shown in Figure 9. Note that the red atoms are Tin and the blue atoms are Niobium [7].

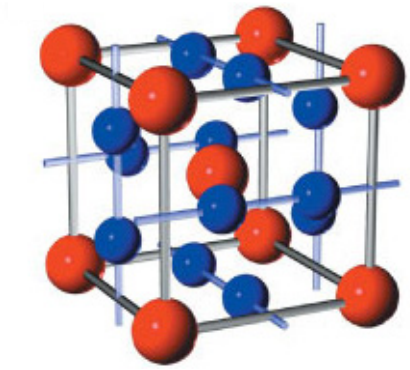

Figure 9: A-15 Structure of Nb_3Sn

Due to its brittle nature, the components of Nb_3Sn must be wound first around the magnet and then treated with heat to form the superconducting compound. There are three main processes to do this: the Bronze Process, Powder in Tube Process (PIT), and the Internal Tin Process. Diagrams of these are shown in Figure 10.

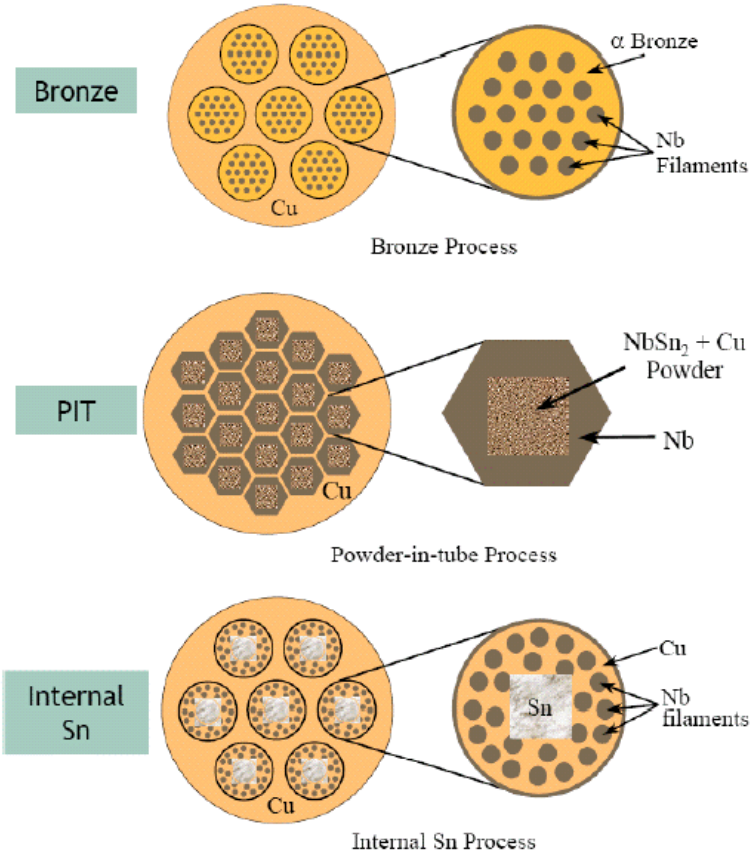

Figure 10: Common Nb_3Sn Production Techniques

In the Bronze Process, filaments of Niobium are inserted into a Bronze matrix containing up to 13.5 wt% Tin and then surrounded by Copper. After appropriate heat treatments, the Tin from the bronze diffuses into the Niobium, forming the Nb_3Sn compound.

In the Powder in Tube (PIT) Process, a ductile form of the Niobium Tin alloy ($NbSn_2$) is inserted inside of a Niobium tube, which is surrounded again by Copper. After appropriate heat treatment, Nb_3Sn is formed within the Copper matrix.

Finally, in the Internal Tin Process, Tin is placed in a Copper matrix and surrounded by Niobium filaments. After appropriate heat treatments, the Tin diffuses into the Niobium to form Nb_3Sn within a Copper matrix. This process has led to the Modified Jelly Roll (MJR) and Restacked Rod (RRP) processes [5].

2.3.2.2 Thermo-Magnetic Instabilities and Measurement

The second, and more demanding, problem with Nb_3Sn is that thermo-magnetic instabilities (or flux jumps) cause the magnet to quench well below the expected critical current density. Flux jumps are detected in tests by a spike in a voltage versus time signal taken from the magnet. In order to study these flux jumps, a test facility called the Vertical Magnet Test Facility (VMTF) was created at Fermilab with the general set-up shown in Figure 11 [8].

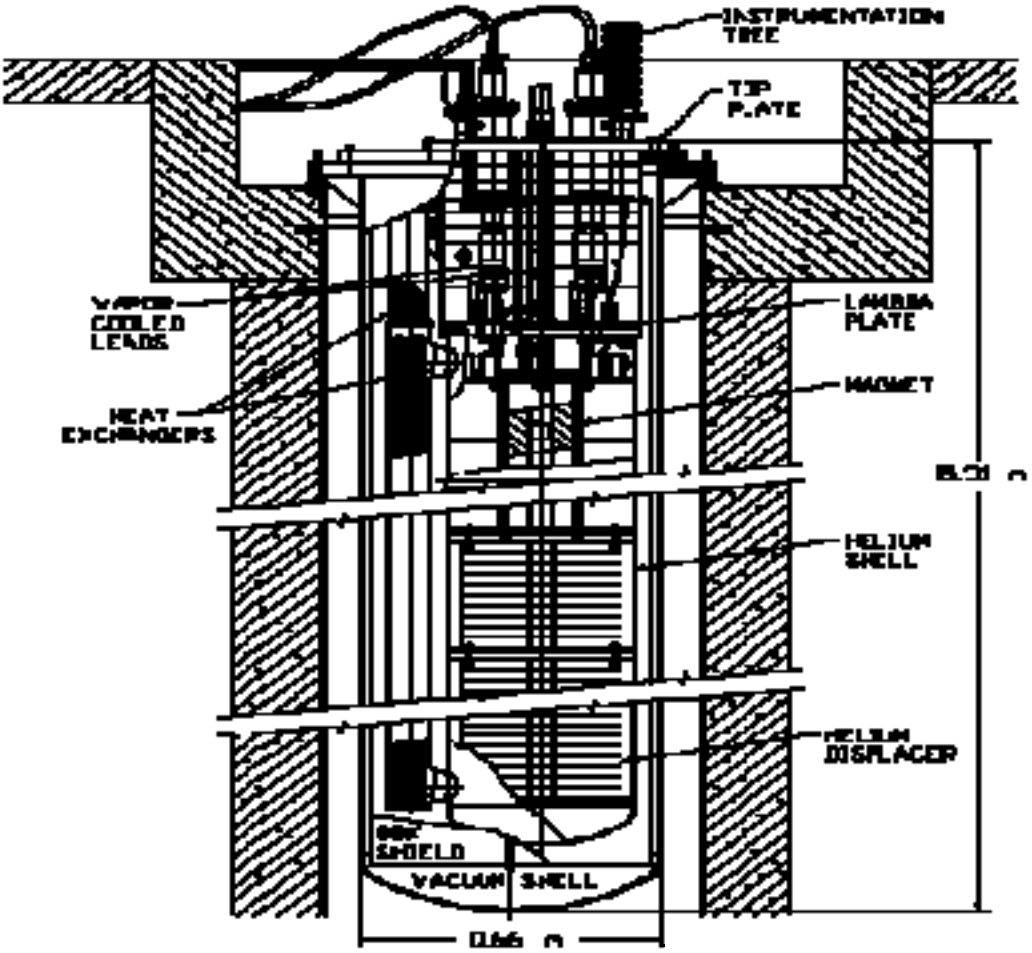

Figure 11: VMTF Dewar

VMTF is a cryostat in the floor of Industrial Building 1 in the Technical Division that allows users to cool a magnet to superconducting temperatures, run current and/or applied magnetic field through the magnet, and then record the results. The program used to record the results is called the Voltage Spike Detection System (VSDS) and was designed by Bernardo Bordini and Sandor Feher ([9] and [10]). The program, written in LabVIEW, takes half second snapshots of the voltage outputted by the VMTF and if the maximum voltage in that window exceeds a threshold set by the user, saves that snapshot; the program then saves all of the snapshots in a single file. Then another LabVIEW program divides that single file into its individual snapshots once again. From here, prior to the summer of 2007, it was necessary for a data analyst to go through each file by hand to characterize each spike. Because there are roughly 70 tests of each

magnet tested in the VMTF and within those 70 tests, roughly 100 snapshots, this proved a tedious task. However, in the summer of 2007, Said Rahimzadeh-Kalaleh developed a program to automate the analysis process called the *Autonomous Voltage Spike Analysis Program* (AVSAP). The Graphical User Interface (GUI) for this program, written by Conor Donnelly, is shown in Figure 12.

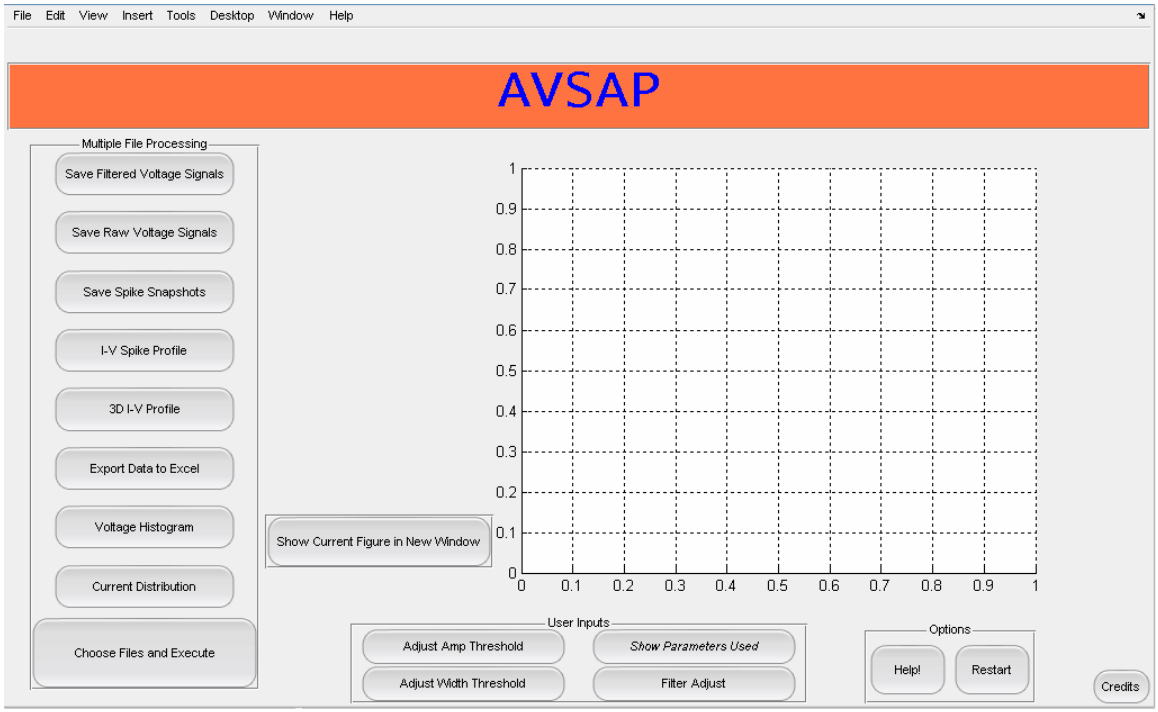

Figure 12: AVSAP GUI

The following is the result of the data analysis, performed with AVSAP, of a magnet named TQC01b.

3. Results and Discussion

This section reports the findings of a voltage spike analysis that was performed on TQC01b, which was tested in July and August 2007 at Fermilab in VMTF.

3.1 Magnet Description

TQC01b is a hybrid of the two best performing coils of TQC01 and a TQS magnet. Figure 13 shows the configuration of these coils that creates the overall structure of TQC01b.

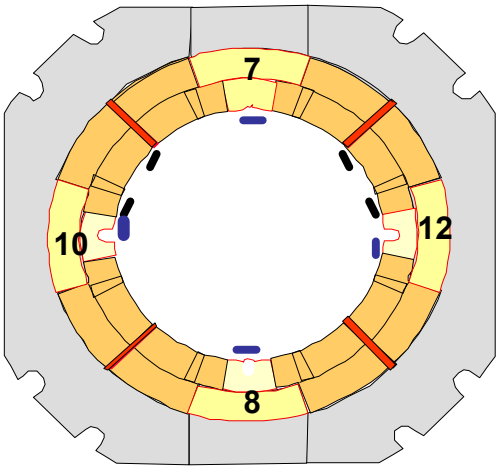

Figure 13: Schematic Cross-Section of TQC01b

Coils 7 and 8 were coils built by Lawrence Berkeley National Laboratory (LBNL) for a TQS magnet and coils 10 and 12 were taken from TQC01, which was built by Fermilab (FNAL).

3.2 Quench Summary

The testing of TQC01b started with 24 training quenches at 4.5 K and 20 A/s. This was followed by a ramp rate study at 4.5 K that lasted 6 ramps. The quench history with the coil in which the magnet quenched is shown in Figure 14 and in table form in Table I.

The short sample limit (SSL in Figure 14) is the theoretical limit of critical current for the magnet in question.

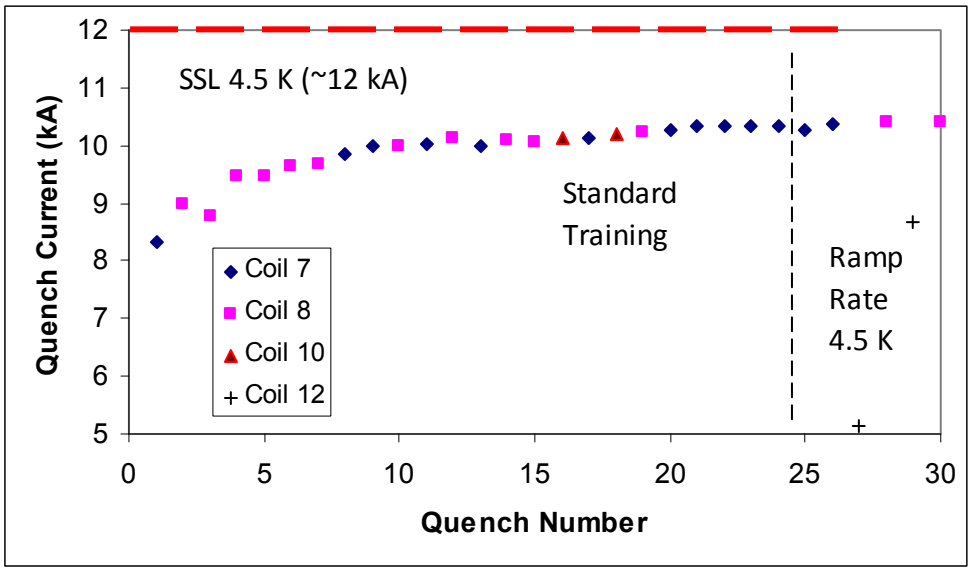

Figure 14: Quench History of TQC01b

Table I: Quench History of TQC01b

Ramp	**Quench**	Coil	Temp (K)	RR (A/s)	Current (kA)	Ramp	**Quench**	Coil	Temp (K)	RR (A/s)	Current (kA)
1	**1**	7	4.5	20	8.338	16	**16**	10	4.5	20	10.138
2	**2**	8	4.5	20	8.984	17	**17**	7	4.5	20	10.13
3	**3**	8	4.5	20	8.779	18	**18**	10	4.5	20	10.198
4	**4**	8	4.5	20	9.4628	19	**19**	8	4.5	10	10.236
5	**5**	8	4.5	20	9.4743	20	**20**	7	4.5	20	10.276
6	**6**	8	4.5	20	9.642	21	**21**	7	4.5	20	10.332
7	**7**	8	4.5	20	9.681	22	**22**	7	4.5	20	10.325
8	**8**	7	4.5	20	9.846	23	**23**	7	4.5	20	10.33
9	**9**	7	4.5	20	9.987	24	**24**	7	4.5	20	10.344
10	**10**	8	4.5	20	9.981	25	**25**	7	4.5	10	10.275
11	**11**	7	4.5	20	10.022	26	**26**	7	4.5	5	10.383
12	**12**	8	4.5	20	10.142	27	**27**	12	4.5	300	5.143
13	**13**	7	4.5	20	9.983	28	**28**	8	4.5	100	10.399
14	**14**	8	4.5	20	10.104	29	**29**	12	4.5	200	8.673
15	**15**	8	4.5	20	10.066	30	**30**	8	4.5	20	10.398

3.3 Voltage Spikes at 4.5 K and 20 A/s

The typical voltage spike population diagram that was generated for the standard training ramps of TQC01b is shown in Figure 15 and with peak magnitudes isolated in Figure 16.

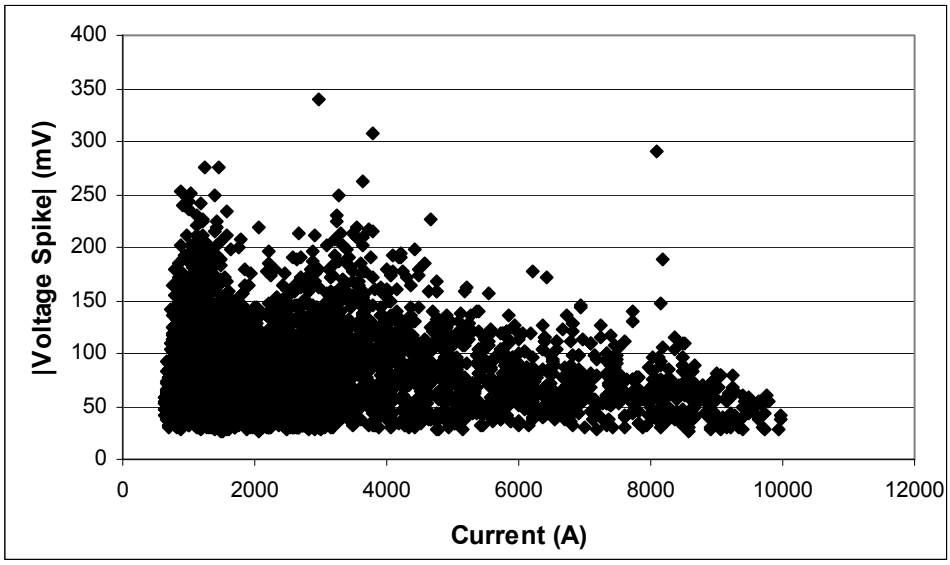

Figure 15: Population Diagram for TQC01b during Standard Training

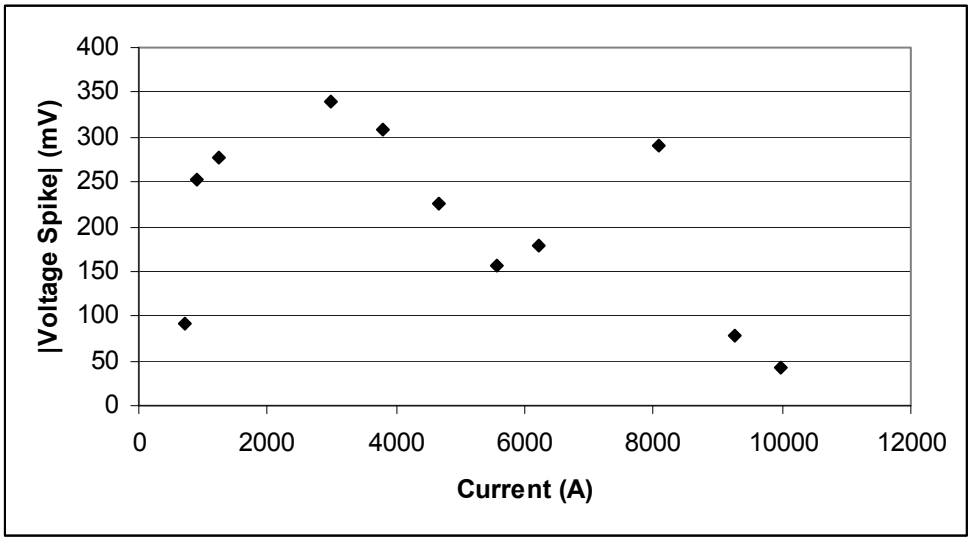

Figure 16: Population Diagram for TQC01b with Peak Voltages Isolated

The general shape of the population diagram with an initial rise followed by an exponential decay is as expected. However, there are more deviations from the general trend in this magnet than was seen in previous magnets. First, there seems to be an absence of density in the 200-350 mV spikes at the 2000 A region. In previous magnets, this region was heavily populated with voltage spikes; in fact, this is the current regime where it is typically expected to see spikes with the greatest magnitude for the entire ramp, but the density is clearly absent here. Moreover, following a smooth decay from about 4000 A to 8000 A, three spikes clearly occurred that had magnitudes as much as 3 times that which is expected at this current level. This caused a secondary maximum in the isolated peak voltages graph, which would lead to a rather ineffective current dependent quench protection threshold should it be employed in similar magnets.

3.4 Statistical Analysis

When the data recorded during standard training is taken as a whole, statistical analysis can be performed on the locations of the spikes with regards to current and voltage spike magnitude. Figure 17 is a histogram, created with MATLAB, that plots number of spikes on the dependent axis and the current at which those spikes occurred on the independent axis.

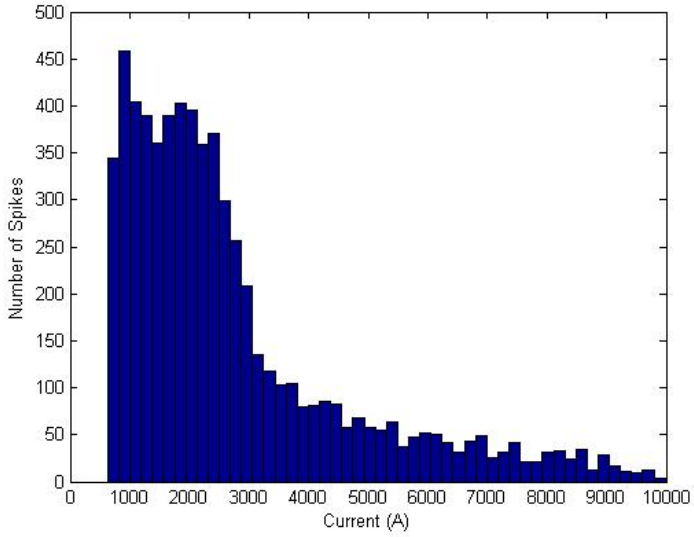

Figure 17: Current Histogram for TQC01b

This is the shape expected of the histogram. Spikes are rarely seen below roughly 600 A, at which point, a huge increase in the number of spikes occurs followed by an exponential decay as current increases from about 2700 A; Figure 17 follows this pattern quite nicely. There were roughly 6450 spikes recorded during standard testing. Using this fact, it can be estimated that roughly 60 % of all the spikes that occurred during the test of this magnet occurred before about 2800 A.

A similar histogram, but with voltage spike magnitude on the independent axis, can also be created for the data and is shown in Figure 18.

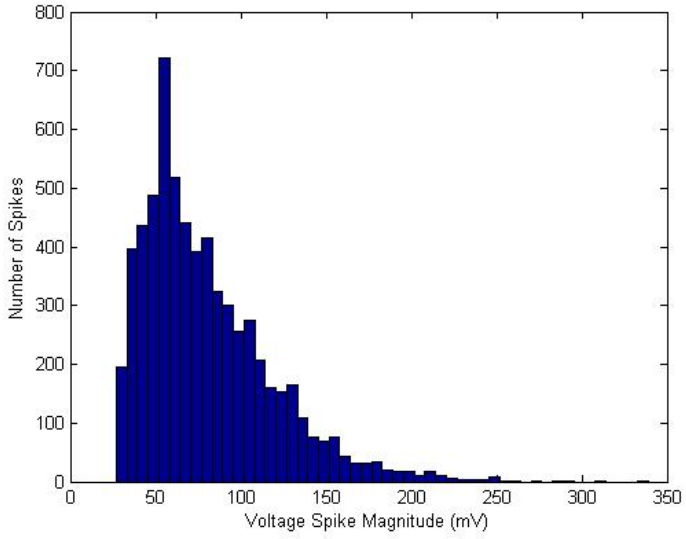

Figure 18: Voltage Spike Magnitude Histogram for TQC01b

Once again, this is the standard shape expected for the distribution. The lack of spikes below 25 mV stems from the fact that a magnitude threshold is used during the operation of the VSDS and AVSAP; spikes do indeed occur below this level, but they are not recorded due to these thresholds. Also, because 6450 spikes occurred during this test, it can be estimated that roughly 35 % of all spikes occurred before the peak voltage spike density of 60 mV had been reached.

The use of AVSAP also allows for another parameter of the spikes to be analyzed, namely the width of the spikes. Because the width of a spike is linked to the change in

flux during a flux jump, this is an important parameter to study. A width histogram is shown in Figure 19.

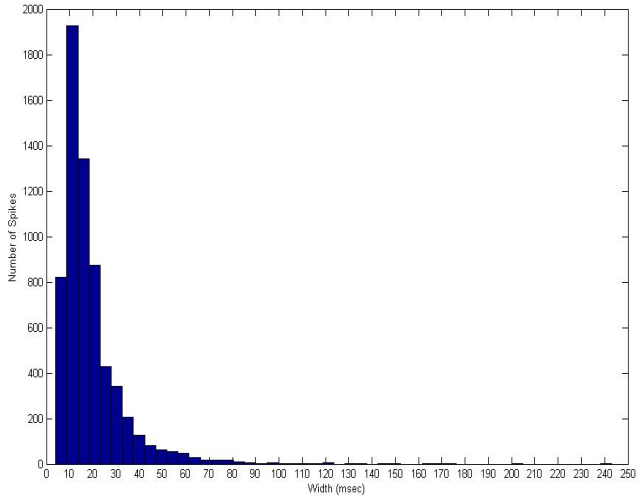

Figure 19: Width Histogram for TQC01b

This profile in Figure 19 is also the expected shape for the distribution of the width of spikes. When taken statistically, the widths in figure 19 are meaningful and show general trends in data. However, it should be noted that the algorithm used to calculate the widths is not always accurate, much of the time it is, but not 100 percent of the time. This is shown in the widths of spikes that are recorded to be in the hundreds of msec. For example, a spike of width 240 msec would take up half of the signal snapshot outputted by the VSDS, which does not occur. Nevertheless, Figure 19 is still a meaningful plot for statistical analysis.

Using the previous three histograms, an estimate of the average changes that happen during a flux jump can be made. If the average magnitude of a flux jump, ~80 mV, and the average width, ~ .02 sec (20 msec), are taken and the general shape of a spike is estimated to be a triangle, a change of about 800 μ webers of flux occurs during a flux jump.

Finally, when combining Figures 17 and 18, the 3D histogram shown in Figure 20 results.

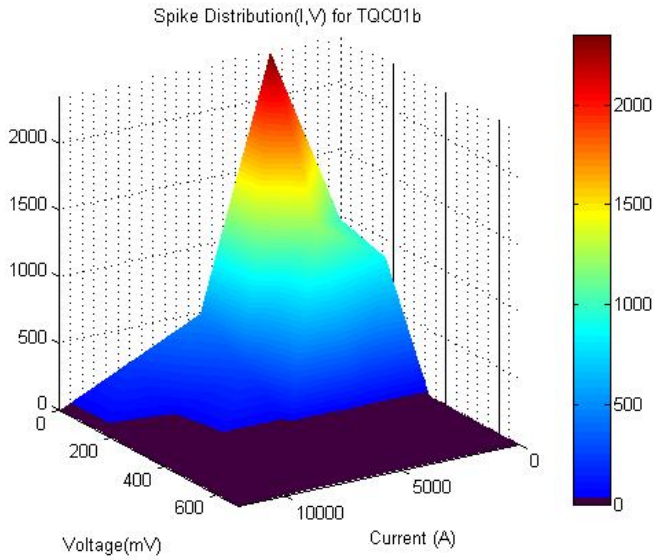

Figure 20: 3D Spike Distribution Histogram

Figure 20 confirms the data presented in Figures 17 and 18. The program for this histogram tends to smooth distributions in the data, which leads to the plot showing a density of spikes where no spikes exist; an example of this is the area around 6000 A and 300 mV in Figure 20. Note also that a black surface indicates that zero spikes at the specified magnitude and current occurred.

3.5 Spike Characterization

During a test, many types of spikes occur; a cursory analysis of these spikes is presented in this section. The typical spike that occurs is characterized by a linear rise followed by an exponential decay. These kinds of spikes occurred at all current levels and an example is shown in Figure 21.

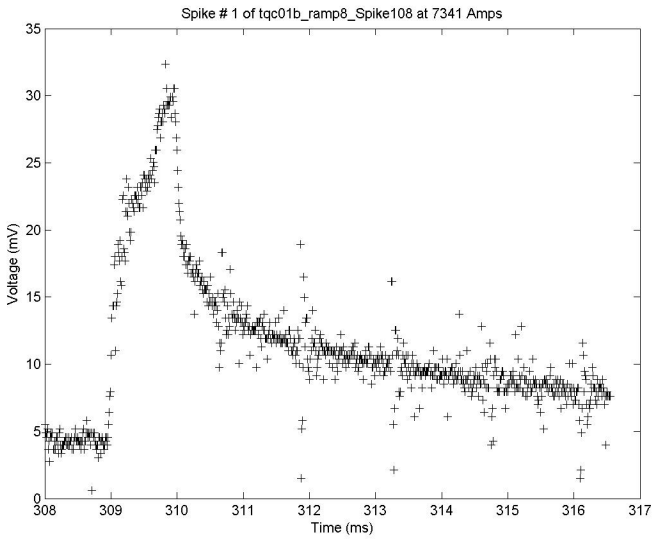

Figure 21: Typical Voltage Spike

At very low currents, i.e. below 1500 A, it is not uncommon to see multiple spikes occur within a very short time frame; this is shown in Figure 22.

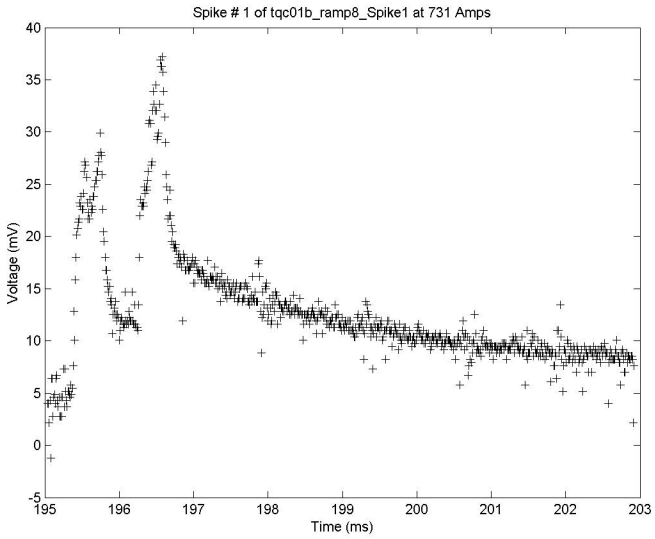

Figure 22: Low Current Spike with Multiple Peaks

As current increases, spikes that seem to oscillate at their peak present themselves (Figure 23).

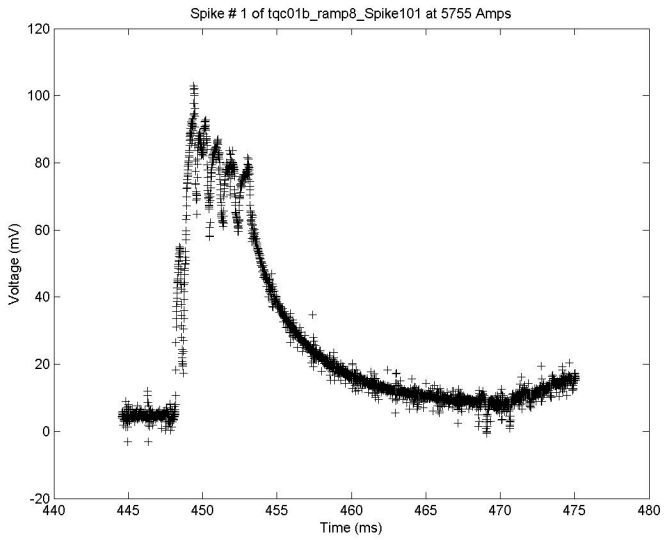

Figure 23: Spike Oscillating about its Peak

As current reaches a few kA, "oscillatory" spikes occur. An oscillatory spike is a spike that has one part of its structure below the y-axis and one part above the y-axis (Figure 24).

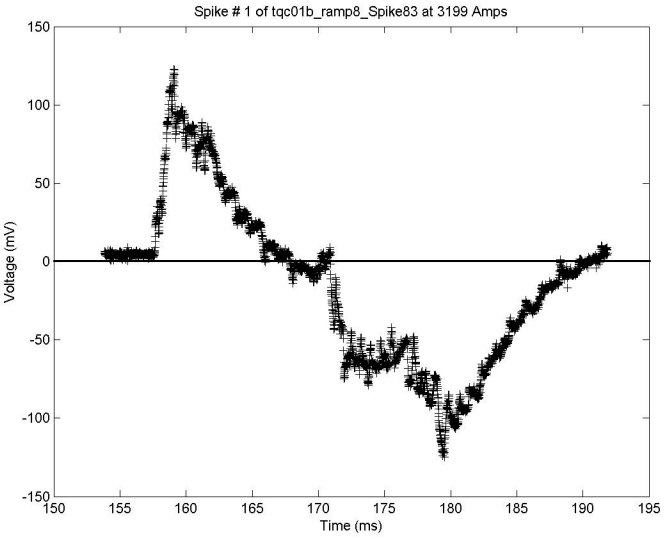

Figure 24: "Oscillatory" Spike

Notice that the spike in Figure 24 spike also seems to oscillate at is peak; it is not uncommon to see a combination of types of spikes occur within a single spike event.

As current reaches the high current regime, the same shapes generally present themselves; the difference in the high current regime is that the spike events tend to be much shorter (a few msec instead of a few tens of msec).

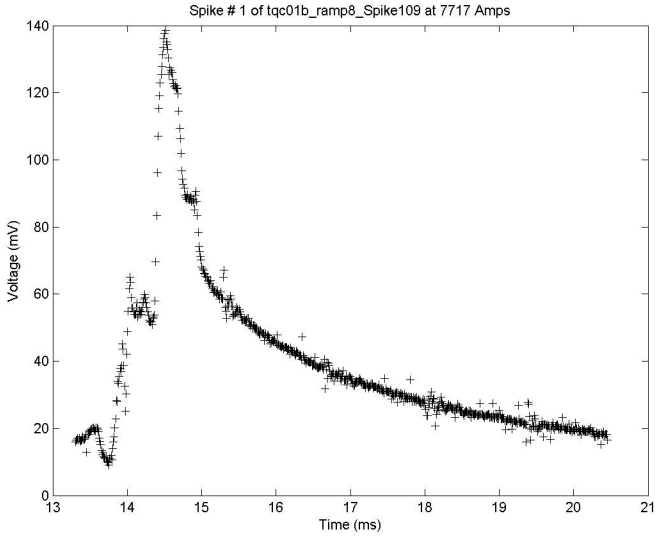

Figure 25: High Current Spike

3.6 Quench Onset

The quenches of interest for TQC01b all occurred in coils 7 and 8. The first three quenches were marked by a fairly smooth increase followed by a plateau in the voltage signal. After the plateau, the quench assumed its normal smooth form; quench 3 occurred in coil 8 and is shown as an example of this (Figure 26).

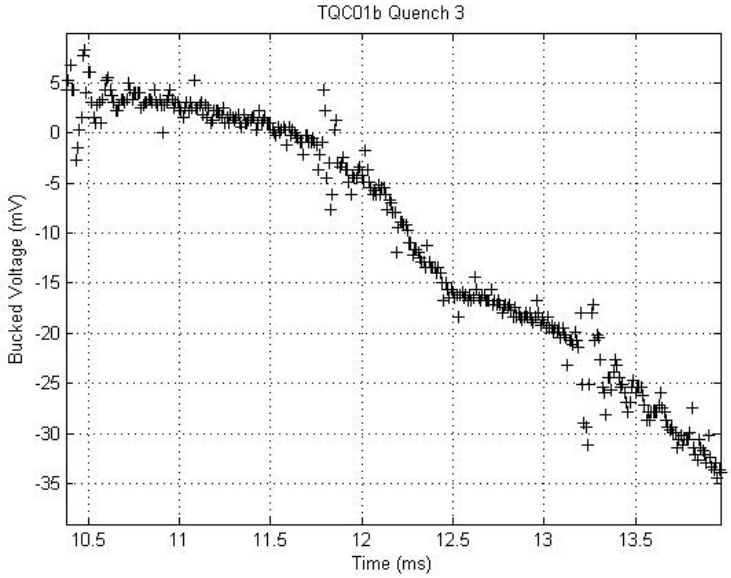

Figure 26: TQC01b Quench 3 Onset (8779 A)

The next 5 quenches all occurred in coil 8; all showed the normal smooth pattern except for quench 4 (Figure 27), which showed a sign of recovery and quench 5 (Figure 28), which showed the opposite concavity than seen in the other quenches in coil 8.

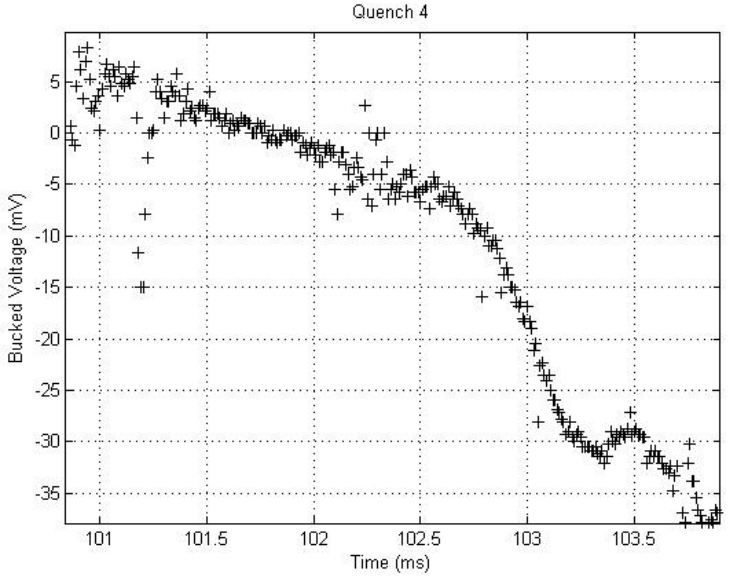

Figure 27: TQC01b Quench 4 Onset (9463 A)

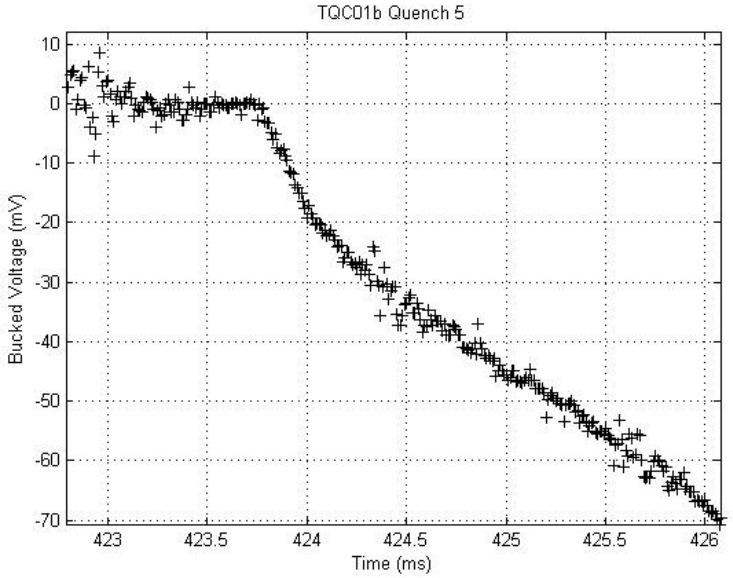

Figure 28: TQC01b Quench 5 Onset (9642 A)

Notice also that in Figure 27 there is a 15 mV voltage spike at about 101.25 msec. This is not the characteristic spike of the power supply that is seen every 1.4 msec. This initial spike occurred in quenches 12, 13, 16, 19, 21, and 22 as well.

Finally, except for the previously mentioned irregular starts to the quench onsets, quenches 14 (Figure 29) through 24 (Figure 30) all exhibited the normal smooth development. It is also interesting to note that quench 14 was the first quench that reached the 10 kA regime.

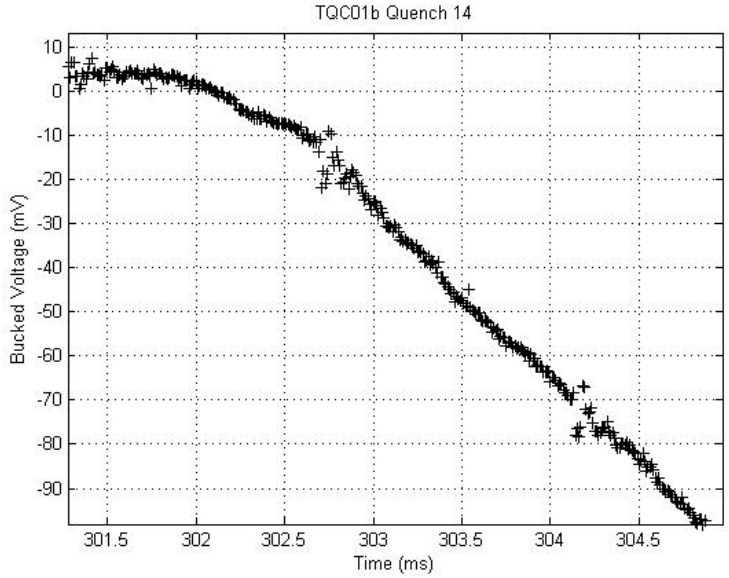

Figure 29: TQC01b Quench 14 Onset (10104 A)

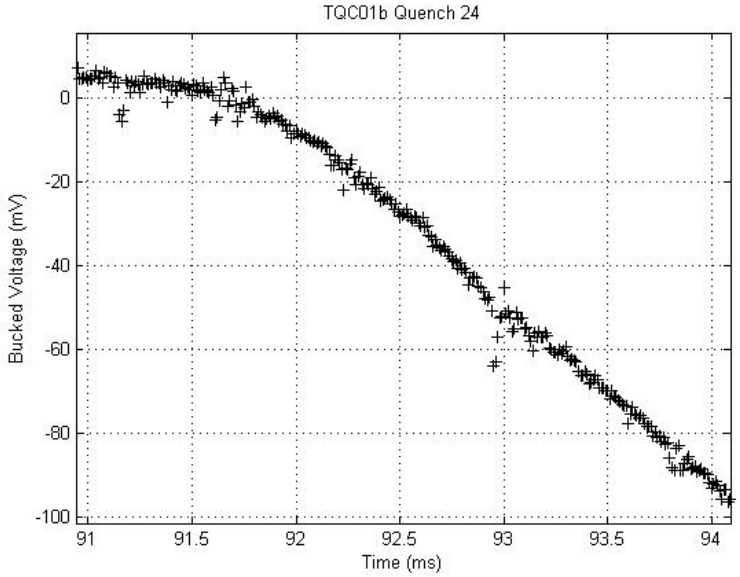

Figure 30: TQC01b Quench 24 Onset (10344 A)

4. Conclusions

The thermo-magnetic instabilities in Nb_3Sn were studied for four separate magnets. Population diagrams of the current dependence of the magnitude of the manifestation of these instabilities, voltage spikes, were created for each of the magnets and statistical

analysis was performed on the acquired data. The characterization of the shapes of the spikes was given a cursory analysis and the onsets of each quench were studied.

A new automated analysis program, AVSAP, was created for faster and more thorough analysis of future data generated by the VSDS in VMTF at Fermilab and was used to analyze one of the magnets in question.

Nb_3Sn still remains the best candidate to replace NbTi as the superconducting material for use in high field accelerator magnets at this time. However, the thermo-magnetic instabilities present in the technology will indeed limit the overall performance of the magnet. Realizing this limitation by creating a current dependent voltage threshold for the magnitude of the voltage spikes seems the safest way to combat these instabilities. With future research into the nature of these instabilities, e.g. their shape and the energy they dissipate, these instabilities could be controlled and the magnet technology could potentially be applied to the LHC upgrade in roughly 10 years and to the International Linear Collider (ILC) in roughly 15 years. More investigation into these instabilities is needed and will be performed.

5. Acknowledgements

This research was conducted in the Technical Division at Fermilab under the Summer Internships in Science and Technology Program. I wish to thank the organizers of the program, especially Dianne Engram and Elliot McCrory, for giving me an opportunity to participate in this terrific program; I truly have learned more than I ever could have imagined possible. I also wish to thank all those in the Technical Division, especially those in IB1 and IB2, for their work that made this research possible. I would be doing a disservice to my parents if I did not give them at least some of the credit for my work this summer; without their support, I would not have even had the opportunity to participate in this program. I wish to thank my associate supervisor, Guram Chlachidze, for always letting me knock on his door to ask him a quick question, no matter what he was doing. Last and certainly not least, I wish to thank my supervisor, Giorgio Ambrosio, whose guidance and example has taught me the true meaning of first-rate research.

References

[1] Callister, William D. *Fundamentals of Materials Science and Engineering: An Integrated Approach 2nd Ed.* Hoboken, NJ: Wiley, 2005.

[2] Fischer, John E. MSE 250 Lecture. Nano-scale Materials Laboratory. University of Pennsylvania. Philadelphia, PA. 24 January 2007.

[3] Eskildsen, Morton R. "Research Interests." University of Notre Dame Department of Physics. 30 July 2007 <http://www.nd.edu/~vortex/research.html>.

[4] Sonneman, F. 30 May 2001. CERN. 30 July 2007. <http://quench-analysis.web.cern.ch/quench-analysis/phd-fs-html/node3.html>.

[5] Bordini, Bernardo. "Thermo-magnetic Instailities in Nb_3Sn Superconducting Accelerator Magnets." (Ph.D Dissertation, Pisa University/Fermilab, 2007).

[6] Johnson, Alan T. University of Pennsylvania. Private Communication. 4 May 2007.

[7] Larbalestier, David, et al. "High T_c Supercondcuting Materials for Electric Power Applications." *Nature*. 414 (2001): 368-377.

[8] T. J. Peterson, K. I. Rabehl, C. D. Sylvester. "A 1400 Liter 1.8 K Test Facility." *Advances in Cryogenic Engineering*. Vol. 43A, New York: Plenum Press, 1998, pp. 541-548.

[9] S. Feher, et al., "Sudden Flux Change Studies in High Field Superconducting Accelerator Magnets", IEEE Trans. Appl. Superconduct., vol 15, no.2 , pp 1591 – 1594.

[10] D. F. Orris et al., "Voltage Spike Detection in High Field Superconducting Accelerator Magnets", IEEE Trans. Appl. Superconduct., vol 15, no.2 , pp 1205 – 1208.

TD-07-015
LARP-July-2007

APPENDIX A: TQS02a Voltage Spike Analysis

C. Donnelly, G. Ambrosio, G. Chlachidze, S. Rahimzadeh-Kalaleh

Contents

1. Abstract

This note reports the analysis of the data recorded by the VSDS (Voltage Spike Detection System) [1] [2] during 68 current ramps of the TQS02a superconducting magnet (LARP Technological Quadrapole). It was found that the voltage spikes at 4.5 K were an order of magnitude larger than the spikes at 1.9 K. Moreover, the shape of each type of spike contained at 4.5 K was given a cursory analysis; four types of spikes were found at low currents, and two types of spikes were found at high currents, with some mixing of types occurring. Following the installation of a physical noise reduction system, data was analyzed and it was found that the vast majority of spikes occurred below 1500 A and had magnitudes below 100 mV. The onset of all available quench onsets was examined and is presented.

2. Quench Summary

For reference, the quench history of TQS02a is presented in figure 1 and in table form in table I.

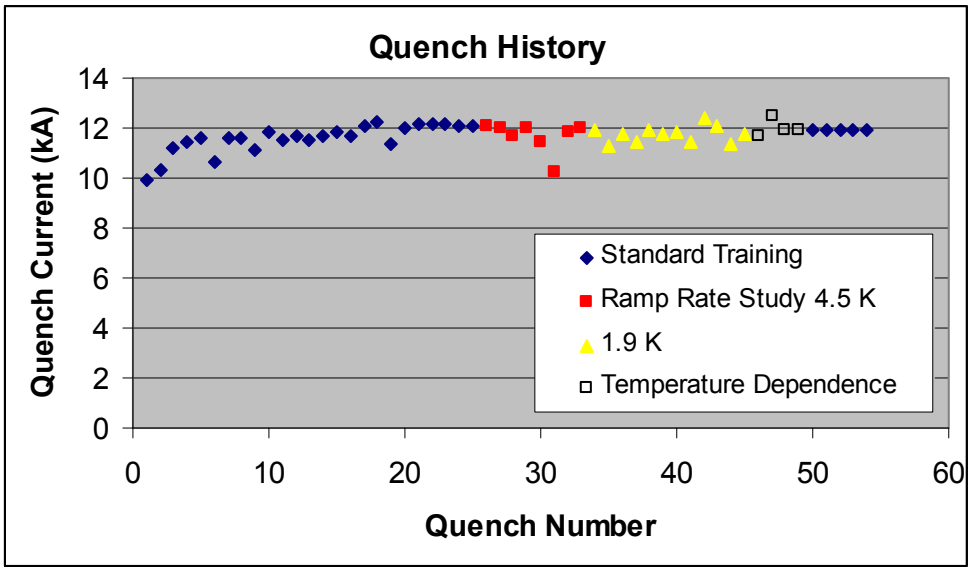

Figure 1: Quench History of TQS02a

Table I: Quench History of TQS02a

Ramp #	Quench #	Coil	Temp (K)	RR (A/s)	Current (kA)	Ramp #	Quench #	Coil	Temp (K)	RR (A/s)	Current (kA)
1	**1**	21	4.5	20	9.9017	29	**27**	21	4.5	40	11.9642
2	**2**	21	4.5	20	10.3212	30	**28**	21	4.45	80	11.714
3[a]			4.5	20	1.7366	31	**29**	21	4.45	10	12.011
4	**3**	22	4.5	20	11.161	32	**30**	21	4.5	100	11.407
5	**4**	20	4.5	20	11.44	33	**31**	21	4.5	120	10.217
6	**5**	20	4.5	20	11.575	34	**32**	21	4.5	60	11.839
7	**6**	21	4.5	20	10.634	35	**33**	21	4.5	5	11.963
8	**7**	22	4.5	20	11.637	36	**34**	21	1.9	20	11.937
9	**8**	20	4.45	20	11.5992	37	**35**	21	1.9	20	11.252
10	**9**	20	4.5	20	11.126	38	**36**	21	1.83	20	11.77
11	**10**	20	4.45	20	11.8456	39	**37**	21	1.82	20	11.439
12[a]			4.45	20	1.949	40	**38**	21	1.9	20	11.941
13	**11**	20	4.5	20	11.495	41	**39**	21	1.91	20	11.731
14	**12**	20	4.5	20	11.7	42	**40**	21	1.89	20	11.844
15	**13**	20	4.5	20	11.515	43	**41**	21	1.9	20	11.411
16	**14**	20	4.5	20	11.696	44	**42**	21	1.86	20	12.383
17	**15**	20	4.5	20	11.802	45	**43**	21	1.94	20	12.045
18	**16**	20	4.5	20	11.71	46	**44**	21	1.92	20	11.374
19	**17**	21	4.5	20	12.069	48	**45**	21	1.9	20	11.741
20	**18**[b]		4.5	20	12.269	49	**46**	21	2.08	20	11.716
21	**19**	21	4.5	20	11.378	50	**47**	20	2.17	10	12.463
22	**20**	21	4.5	20	11.97	51	**48**	20	2.95	20	11.957
23	**21**	21	4.5	20	12.162	52	**49**	21	4.42	20	11.933
24	**22**	21	4.5	20	12.146	53	**50**	21	4.44	20	11.935
25	**23**	21	4.4	20	12.139	54	**51**	21	4.44	20	11.934
26	**24**	21	4.5	20	12.11	55	**52**	21	4.44	20	11.925
27	**25**	21	4.42	20	12.071	57	**53**	21	4.45	20	11.917
28	**26**	21	4.5	5	12.0496	68	**54**	21	4.45	20	11.927

3. Voltage Spikes at 4.5 K

At currents below 2000 A, spikes on the order of a few volts were not uncommon. A maximum voltage spike of 4.2 V at 1820 A was observed during ramp 64. The general profile of the voltage spike magnitude versus current seems to show a steep increase followed immediately by a consistent exponential decay. This is shown in figure 2 below and more clearly with maximum peaks isolated in figure 3. Note that this same pattern was seen in TQC01, albeit with peaks more than an order of magnitude smaller.

[a] Ramp 3 and 12 contained spikes that tripped the QDS.
[b] Quench occurred at a coil to coil NbTi junction.

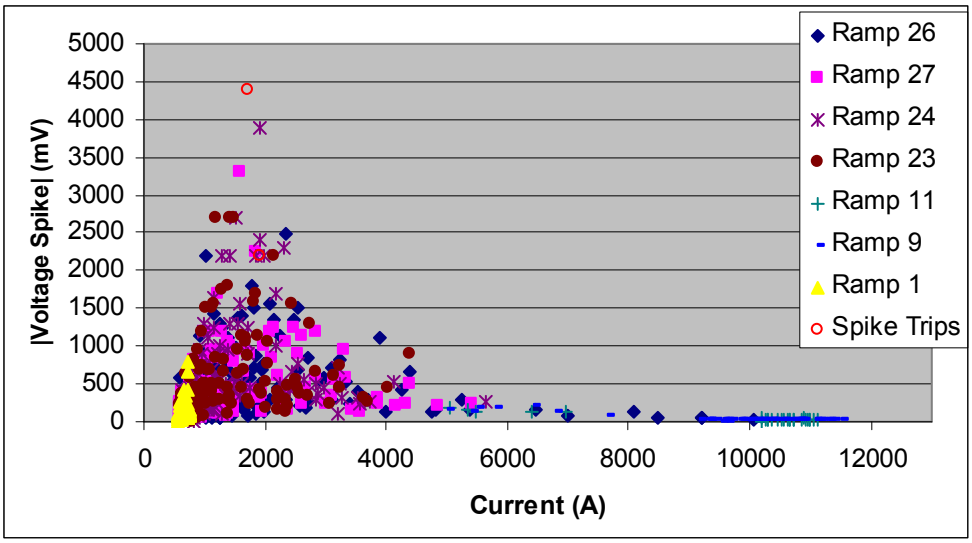

Figure 2: Magnitude of Voltage Spikes versus Current

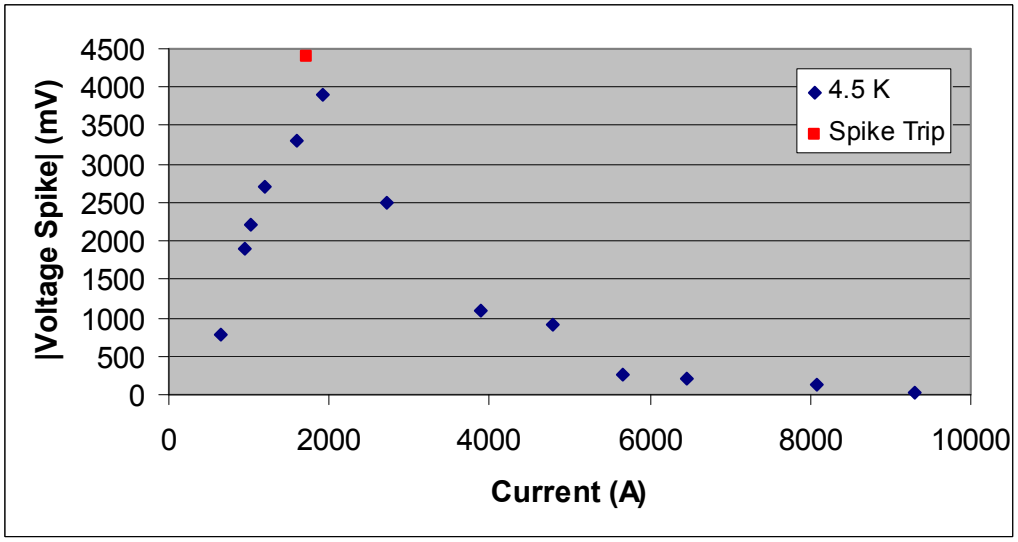

Figure 3: Magnitude of Peak Voltage Spikes versus Current

The voltage spikes can clearly be divided into 2 distinct groups based on peak voltage: above 5000 A and below 5000 A. Because of this, a graph of the spikes above 5000 A is shown in figure 4 below.

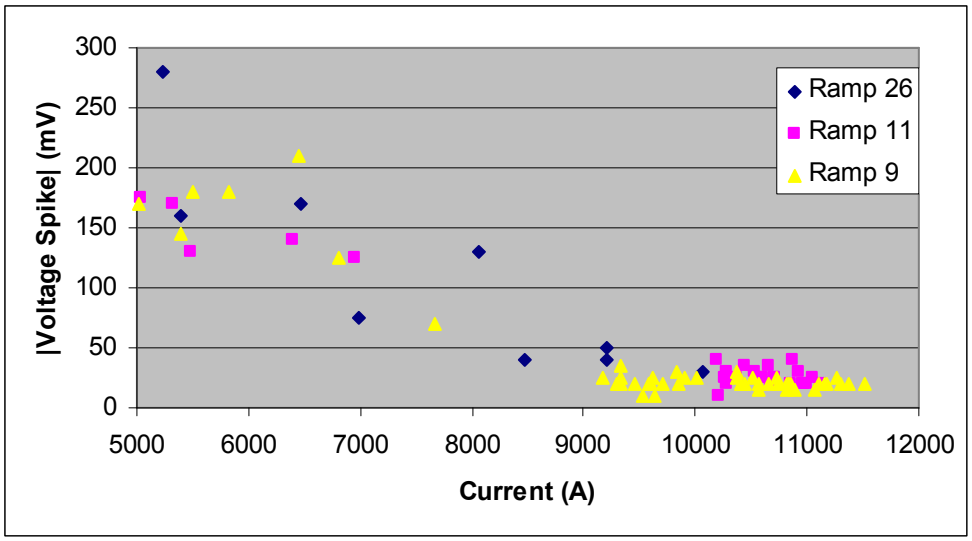

Figure 4: Magnitude of Voltage Spike versus Current for Currents Greater than 5000 A

This close up view of high current spikes shows that the trend of "exponential" decay clearly continues in the high current regime. However, there is a problem with detecting spikes at these currents prior to the installation of the noise reduction system; the noise amplitudes at these currents are typically between 75 and 100 mV with the spikes being less than half this height. The detection of spikes at these currents seems to be a result of the noise crossing the threshold of the VSDS, not the magnitude of the actual spike, so lowering the threshold of the VSDS will not aide in spike detection at these currents. Only approximately 20 % of the 240 "spikes" that the VSDS returned above 5000 A contained actual spikes. In order to confirm that the noise in the high current spikes was similar noise in low current spikes, a Fast Fourier Transform of the noise at each level was performed and the results were quite similar with peak frequencies between 45 and 50 kHz (figures 5 and 6). However, at high current, the magnitude of the peaks was roughly twice that of the low current peaks.

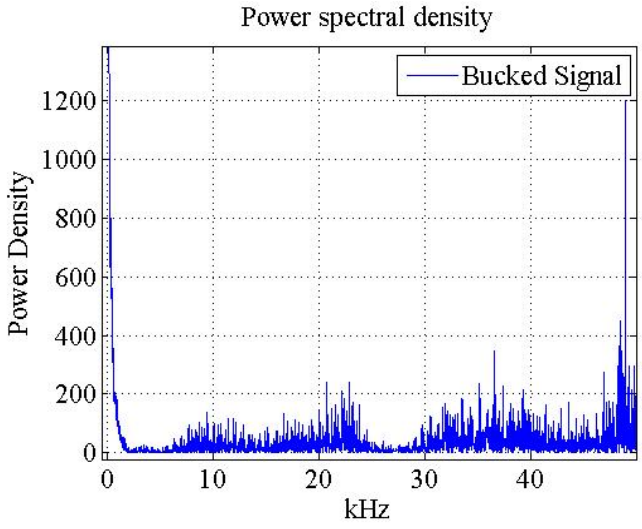

Figure 5: FFT of low current noise

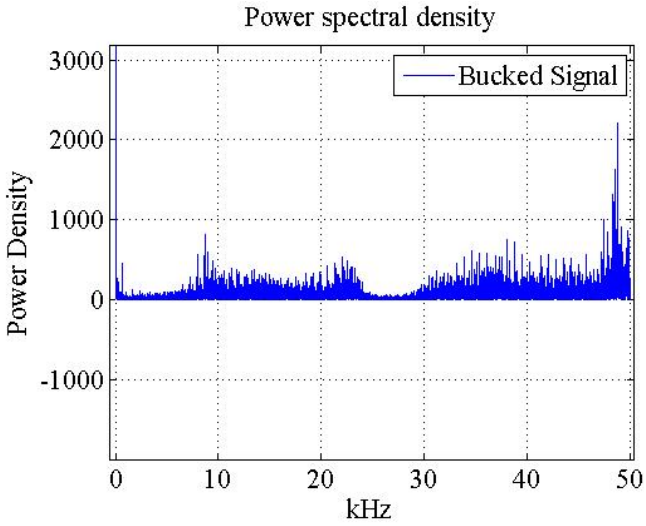

Figure 6: FFT of high current noise

The main difference in the transforms lies in the amplitude of the frequencies, with the high current amplitudes being larger. This result is expected as, visually, the high current snapshots are noisier than the low current snapshots.

4. Spike Characterization at 4.5 K

4.1 Low Current

Once again, the characterization of the spikes can be divided into those seen at low currents and those seen at high currents. At low currents, there are four main categories of spikes, including some that are combinations of two different kinds of spikes. First, the simplest spike is characterized by a linear rise and exponential decay and can occur at any current in the low current (sub 5000 A) regime. It is shown in figure 7 below.

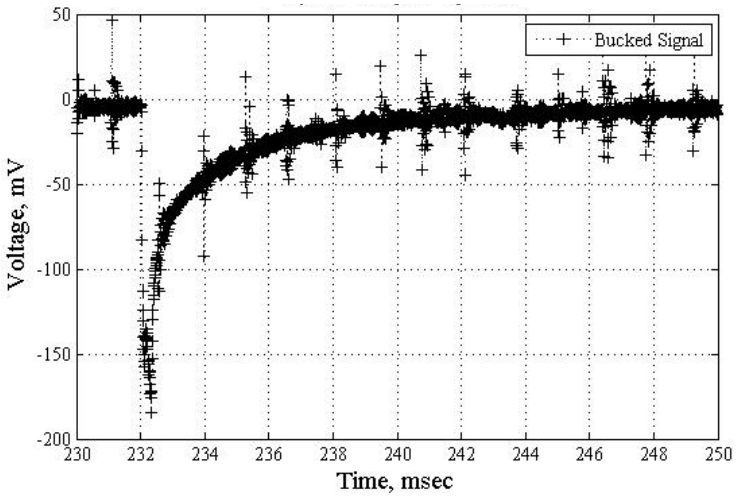

Figure 7: Typical Low Current Spike (670 A)

Notice the periodic noise that is present in each of the snapshots, such as at 238 ms in figure 7. This is the characteristic noise of the power supply and occurs about once every 1.4 ms. At very low currents, below about 1500 A, multiple distinct consecutive spikes, like those in figure 8 below, could be seen.

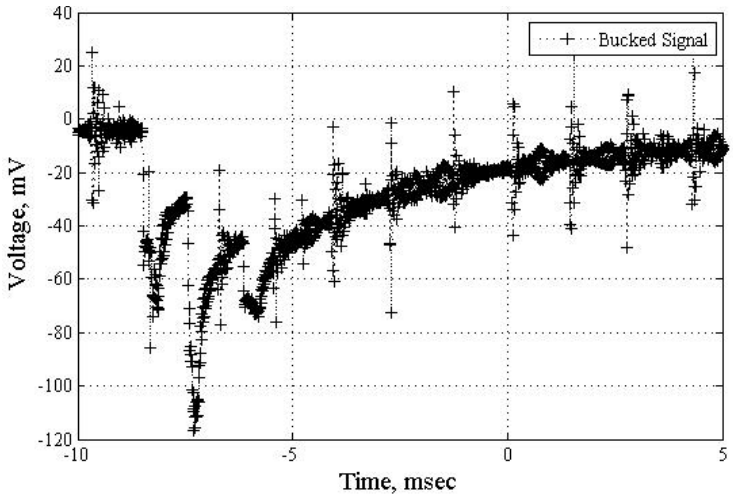

Figure 8: Distinct Consecutive Spikes (570 A)

As current is increased, the distance between distinct consecutive spikes became shorter and the signal appeared to oscillate at its peak. (Figure 9)

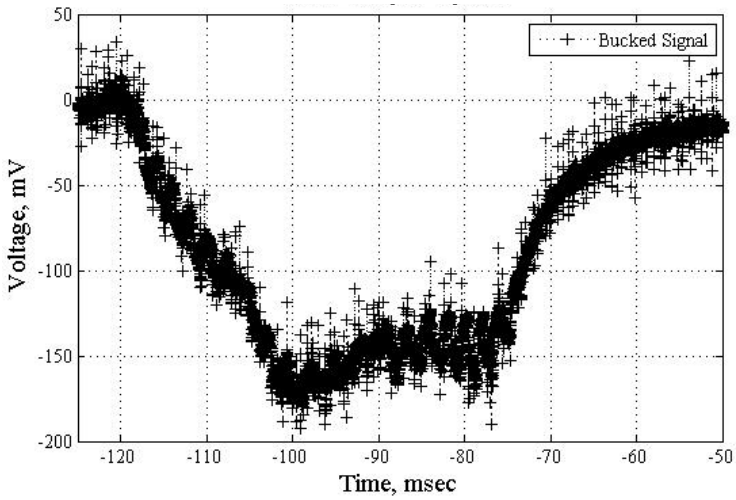

Figure 9: Spike Oscillating at Its Peak (2610 A)

The final type of spike has a portion of its amplitude both above and below the y-axis and is shown in figure 10 below.

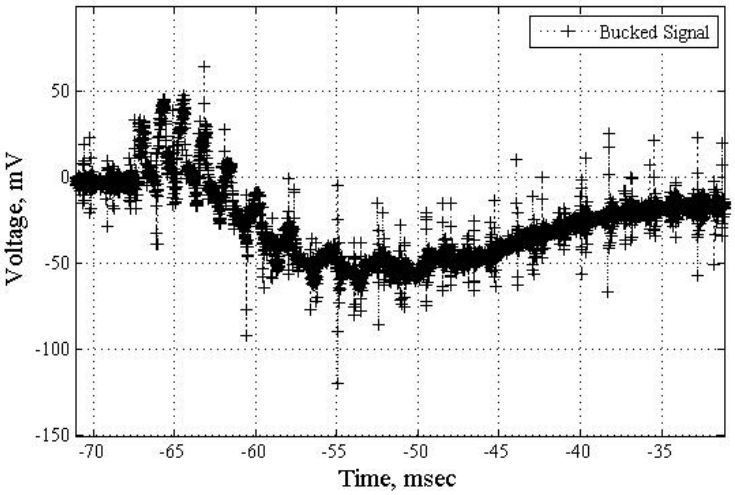

Figure 10: Spike Oscillating about Peaks and Y-axis (4790 A)

Notice how this spike contains two different categories of spikes; this is not an uncommon phenomenon to see at these current levels.

4.2 High Current

At high currents, there are only two types of spikes; however, these are present throughout the 5000 A + regime. The most common spike (Figure 11) is a scaled down version of figure 7; it is characterized by a linear rise and exponential decay.

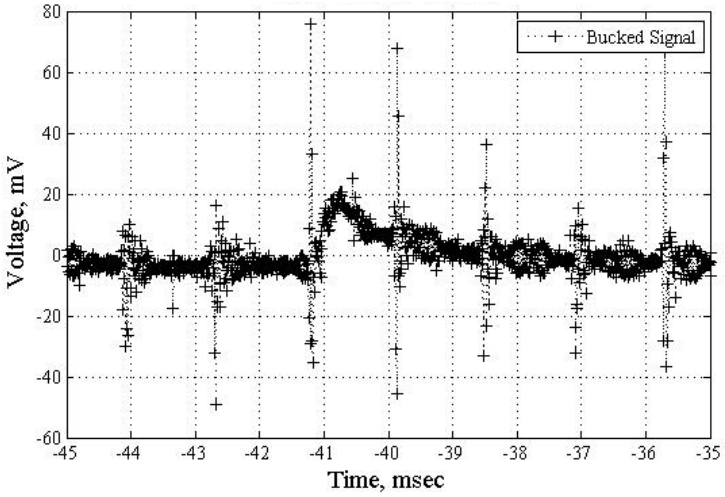

Figure 11: Typical High Current Spike (11150 A)

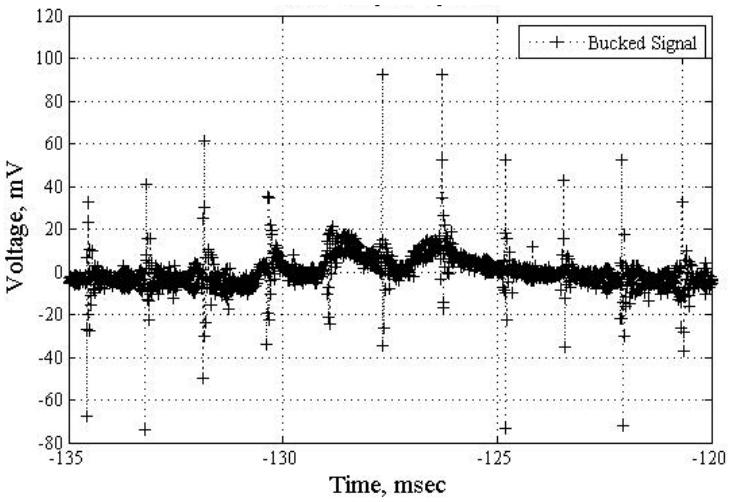

Figure 12: High Current Spike Oscillating at Peak (11120 A)

The second kind of high current spike oscillates around a value that lies above (or below for a negative spike) zero. (Figure 12)

It is also important to note that the inherent noise in the sample was greater in the high current samples than in the low current samples, as shown in figures 13 and 14.

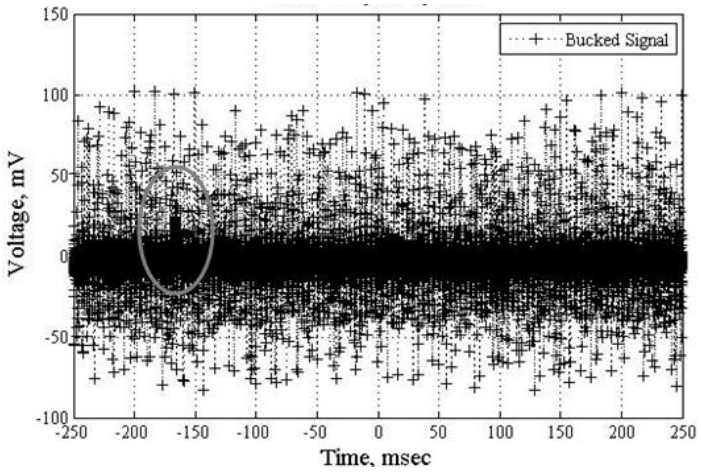

Figure 13: Typical Spike and Noise at High Currents (11050 A)

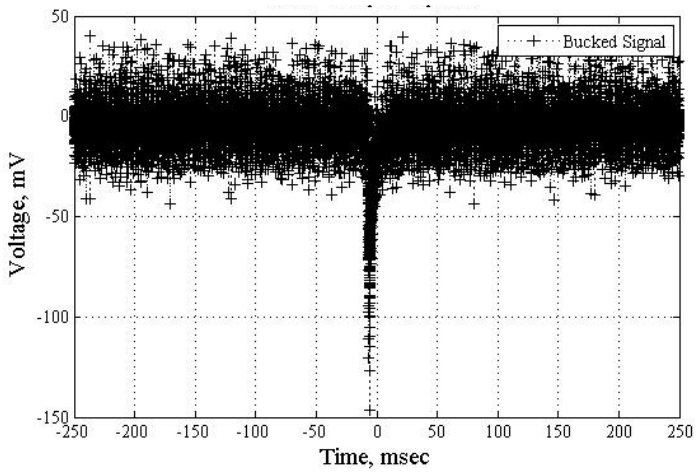

Figure 14: Typical Spike and Noise at Low Currents (1300 A)

5. Voltage Spikes at 1.9 K

As with the spikes at 4.5 K, the magnitude of each voltage spike at 1.9 K was plotted against the current at which it occurred; the result is shown in figure 14 below.

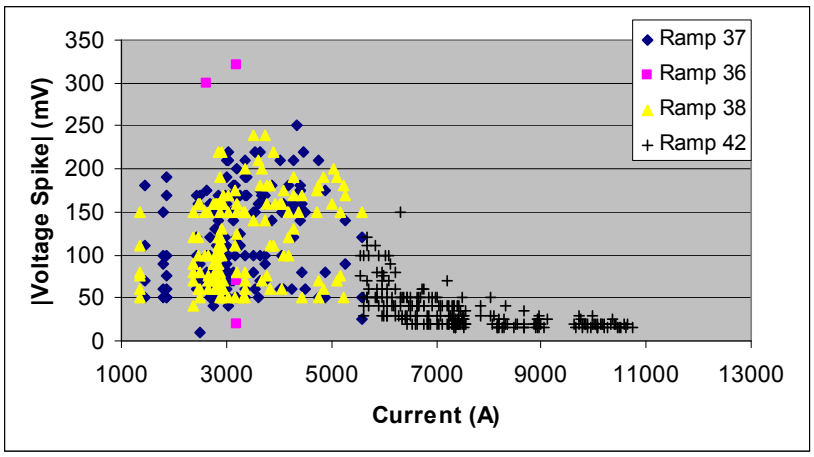

Figure 14: Magnitude of Voltage Spike versus Current Profile at 1.9 K

Once again, the trend is easier to see when the peak voltages at selected currents are isolated and plotted. (Figure 15)

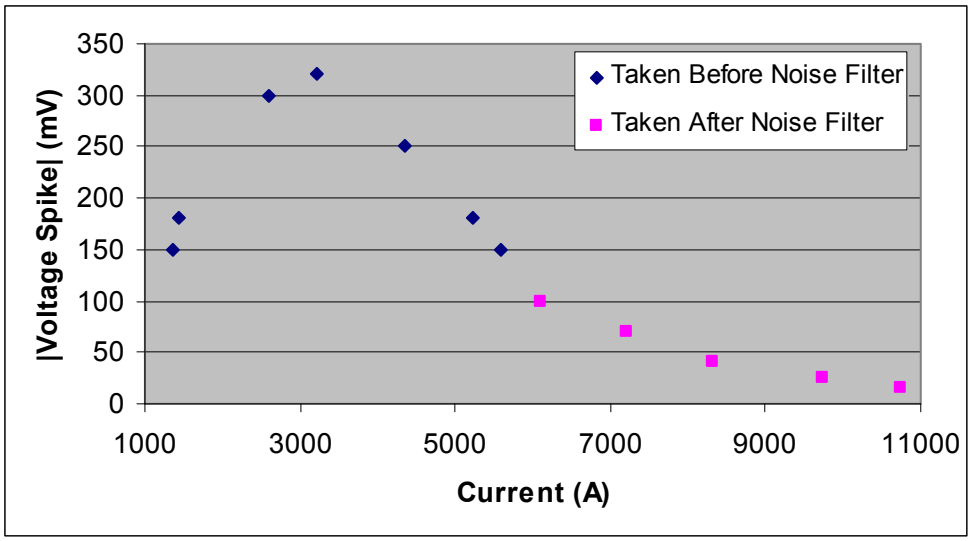

Figure 15: Peak Isolated Profile at 1.9 K

The profile stopped at about 5600 A before a noise filter was installed because, as with the high current scenario at 4.5 K, the threshold for the VSDS system was set too high for the magnitude of spikes present. After the filter was installed, it was possible to lower the threshold and therefore detect the smaller spikes at higher currents.

In order to better understand the spike behavior at high currents at 1.9 K, the VSDS threshold was lowered for ramp 42 to detect more spikes. The spike profile for ramp 42 is shown below.

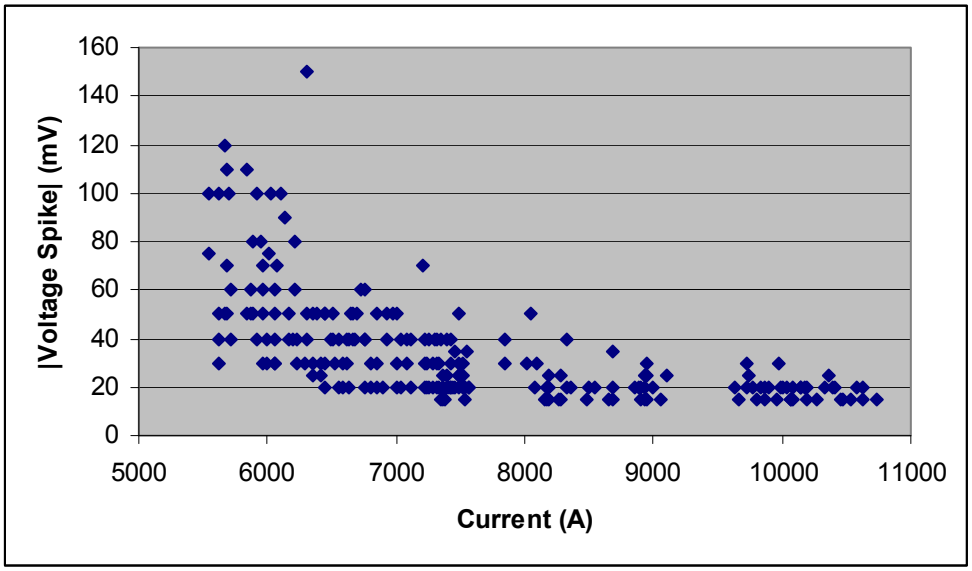

Figure 16: Profile for Ramp 42

It is clear that the exponential decay that was expected at high currents was indeed present for TQS02a. It is also important to note that above 7400 A, roughly 40 % of the events detected by the VSDS were tripped by noise and did not contain any true spikes.

This problem was remedied by the installation of the aforementioned physical noise reduction system and the results of that study are presented later in this report.

6. Comparison of 1.9 K and 4.5 K Tests

The difference in magnitude of the voltage spikes can best be seen by plotting figures 3 and 15 on the same axes: shown in figure 17 below.

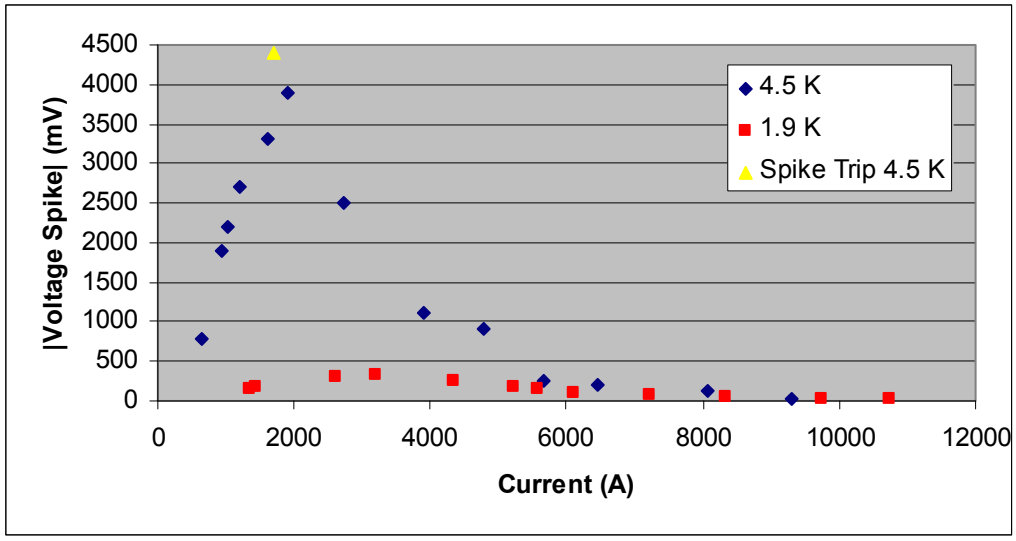

Figure 17: Magnitude of 1.9 K and 4.5 K Spikes

It is obvious that the spikes at 4.5 K are roughly and order of magnitude greater than the spikes at 1.9 K up to about 5000 A, the end of the low current regime. However, at current above roughly 5600 A, the magnitude of the voltage spikes at both temperatures was of the same order of magnitude.

8. Spike Analysis with Low Noise

On June 20, 2007, a physical noise reduction system ("noise filter" in the following) was installed on the Vertical Magnet Test Facility (VMTF) at Fermilab. The filter showed immediate improvements in the output of the VSDS as it reduced the noise at high currents to levels below the magnitude of the actual spikes. Figures 18 and 19, respectively, show the VSDS output before and after the installation of the noise filter.

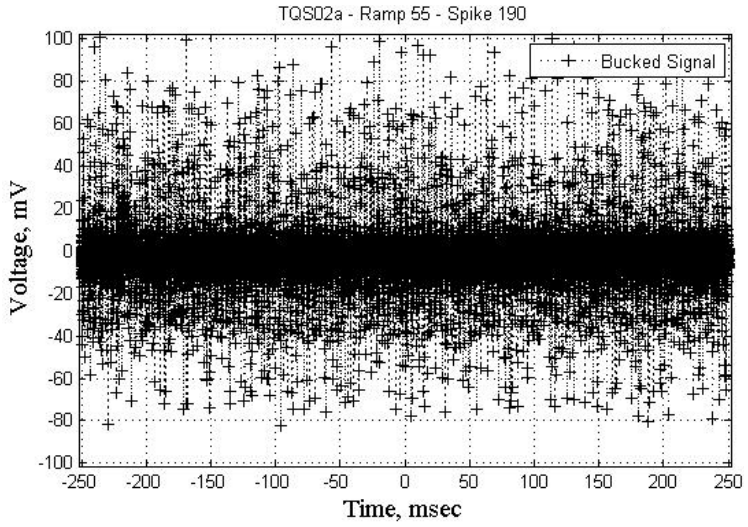

Figure 18: Typical High Current Spike (10.95 kA) Before Noise Filter

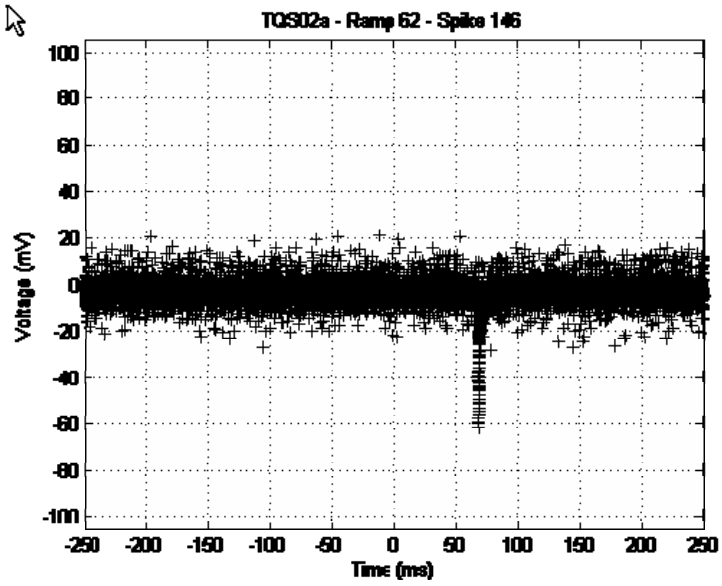

Figure 19: Typical High Current Spike (10.87 kA) After Noise Filter

After the installation of the noise filter, the magnitude of the spikes was clearly greater than the magnitude of the noise at high currents. Also, it was noticed that the overall magnitude of high current spikes became apparently greater after the noise filter was installed because the VSDS was triggered by real spikes rather than by noise.

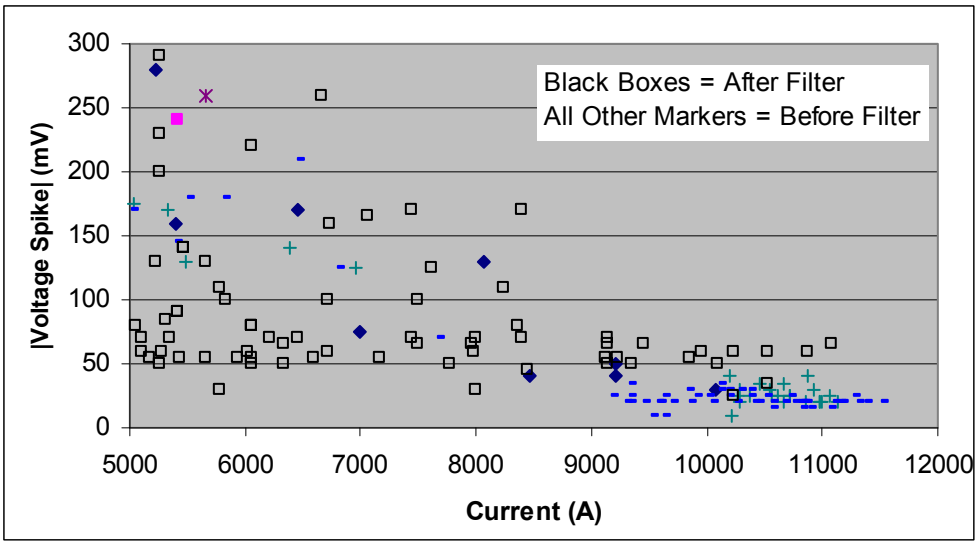

Figure 20: High Current Spikes Before and After Noise Filter Installation

The noise filter also allowed the VSDS to detect spikes at very low currents. Previously, the lowest current at which spikes were recorded was roughly 600 A; however, in the ramps with the noise filter, spikes were detected as low at 300 A (Figure 21).

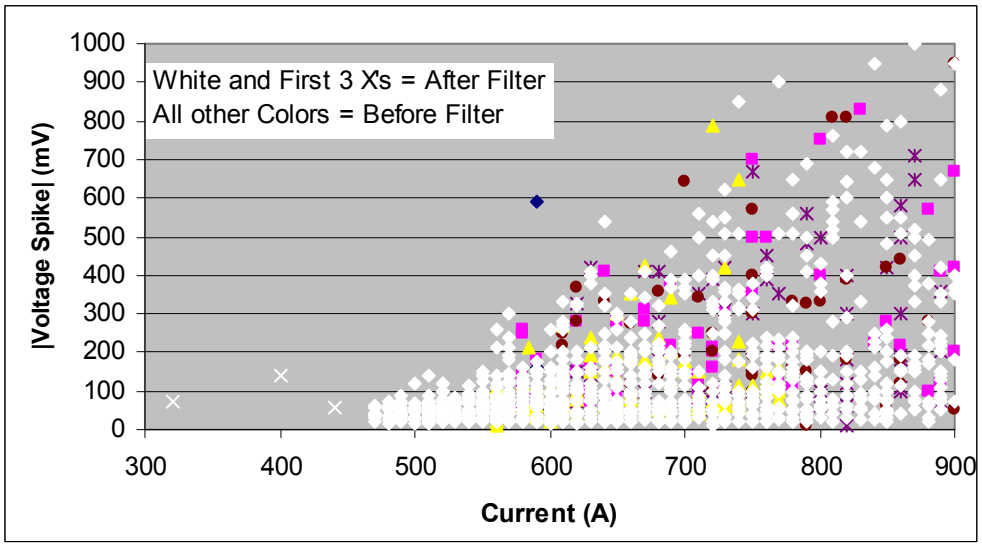

Figure 21: Low Current Spikes Before and After Noise Filter Installation

However, at intermediate currents, the I-V profile for the noise filtered spikes generally fell within the profile established by the pre-filter ramps. The profile with the filtered ramps added is presented in figure 22 below.

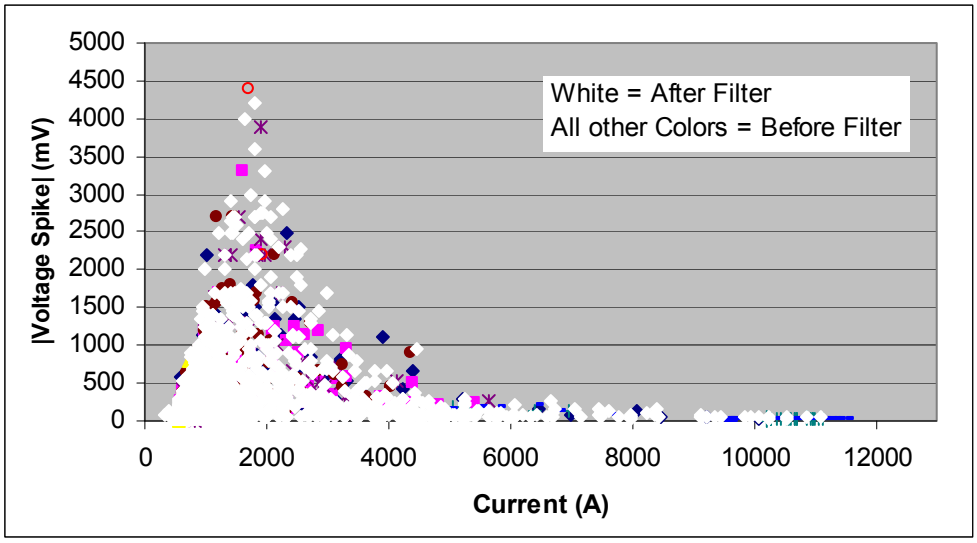

Figure 22: Voltage Spike Profile After Noise Filter Installation

When comparing figure 22 to figure 2, there seems to be a greater density of spike data after the filter was installed. This is a result of the threshold setting on the VSDS. With the high noise samples, the threshold had to be set high enough to prevent noise trips; therefore, smaller spikes were not saved by the VSDS. This led to a greater quantity of filtered spikes being saved by the VSDS.

Since the filtered data was relatively similar to the unfiltered data and since more spikes were saved in the filtered data set, statistical analysis was performed on the filtered data to better understand the voltage spikes and the currents at which they occurred. Figure 23 below is a normalized probability distribution graph, created with Matlab, of the number of spikes that occurred during a ramp versus current.

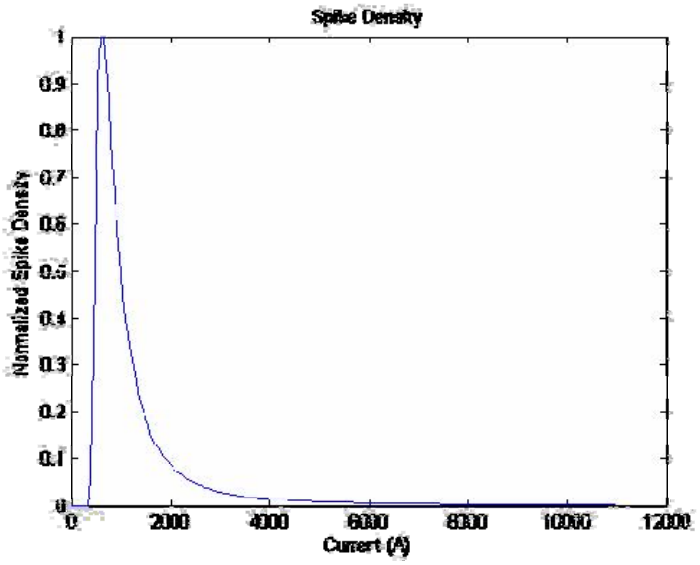

Figure 23: Number of Spikes Distribution

The most interesting point of this graph is that most of the spikes during a ramp occurred before the current reached 1500 A. A similar profile was created for the magnitude of the spikes themselves.

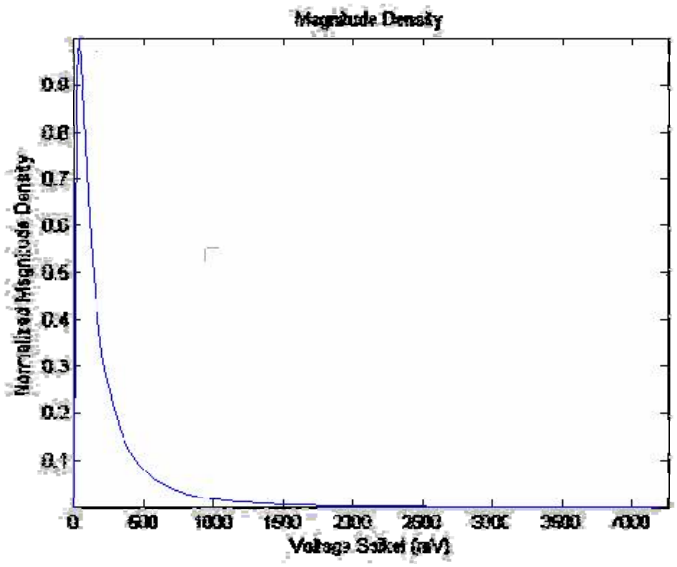

Figure 24: Magnitude of Spikes Distribution

This figure is even more definitive than the previous figure; it clearly shows that most of the spikes that occur during a ramp are below 150 mV in magnitude. Putting these two distributions together leads to the histogram presented in figure 25 below[c].

[c] The Matlab code for this histogram was adapted from "2D Histogram" by Murphy O'Brien, which is available on the Matlab File Exchange.

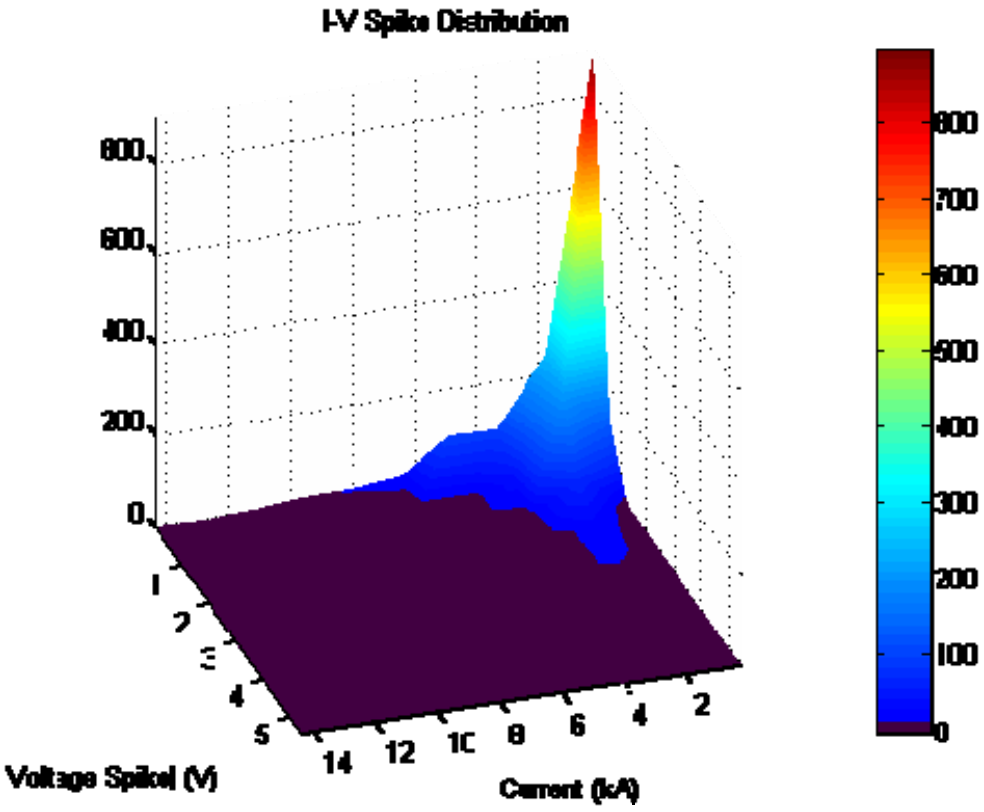

Figure 25: Histogram of Voltage Spike and Current Data

In this plot, a redder surface indicates a greater density of spikes at that current and voltage spike magnitude, a bluer surface indicates a lesser density of spikes, and a black surface indicates a density of zero. The z-axis is unitless and is normalized to the greatest spike density. This reinforces the previous two figures, as the vast majority of spikes that occur at low current have a low voltage spike magnitude.

9. Quench Onset

At this point in time, only trends can be identified with regards to characterizing the onset of the quenches. Most of the quenches from quench 4 to quench 16 occurred in coil 20 and most of the quenches from quench 17 to the conclusion of testing occurred in coil 21, specifically in B2-B3 and B3-B4 segments.

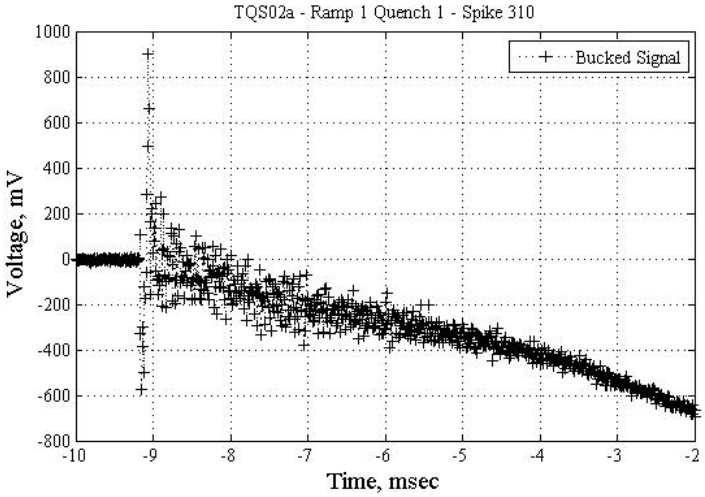

Figure 26: Quench onset of Quench 1 (99017 A)

Figure 26 shows the quench onset of the first quench. The large oscillating spike at about -9 ms (arbitrary zero) has been seen in other magnets and has been interpreted as mechanical movement. Quench 4 showed a slightly similar behavior; however, the starting spike had much smaller amplitude.

The first group of onset quenches, which are the expected form of quench onsets in the case of a normal transition, appeared in quenches 2-18. These are characterized by a generally smooth voltage increase over time; an example is shown in figure 27 below.

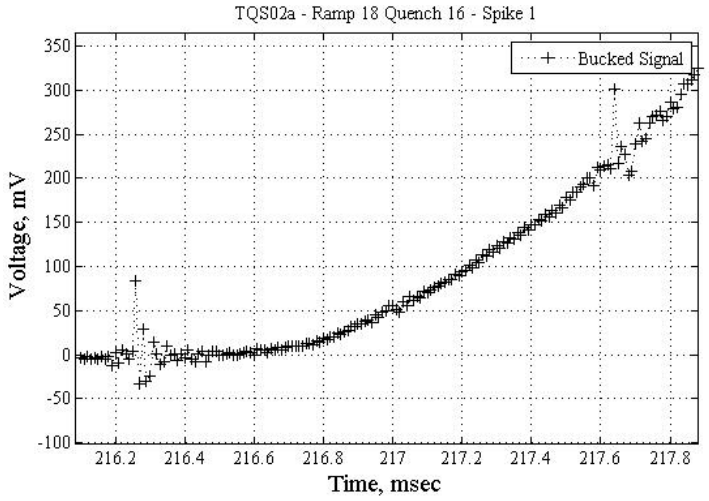

Figure 27: Quench Onset of Quench 16 (11710 A)

Note that the noise in figure 27 at 216.3 ms and 217.7 ms is characteristic of the power supply. Then, quite suddenly, the onset became irregular and also initiated in coil 21. This is shown in figure 28 below.

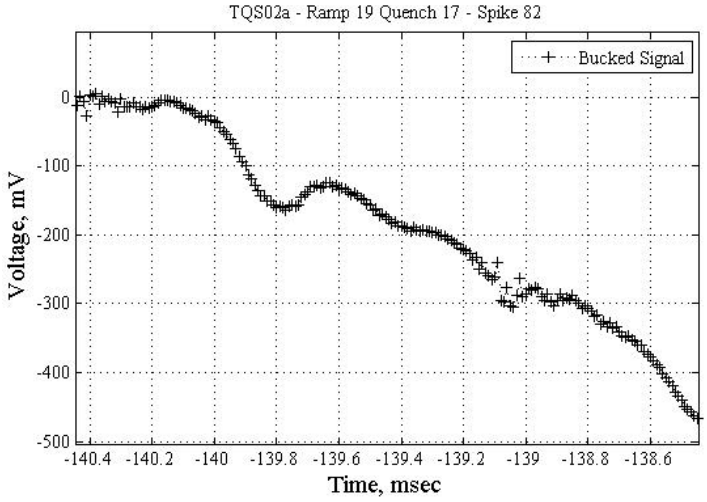

Figure 28: Quench onset of Quench 17 (12069 A)

This pattern continued until quench 21 when the shape of the irregularities changed slightly. (Figure 29) However, the quench began in the same coil and coil segments as quenches 17-20.

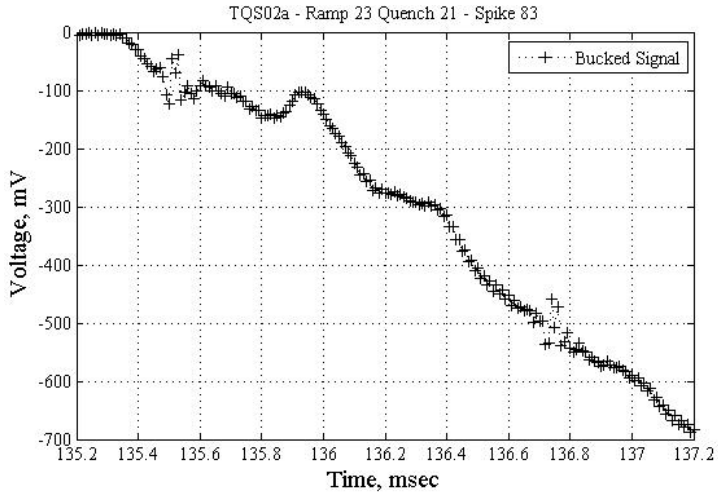

Figure 29: Quench onset of Quench 21 (12162 A)

This continued through quench 25, which ended standard training. Following a ramp rate study, ramps to quench at 20 A/s were performed at 1.9 K (Quenches 36-48). The irregularities seen at 4.5 K were again seen at 1.9 K and the magnet continued to quench in coil 21. (Figure 30)

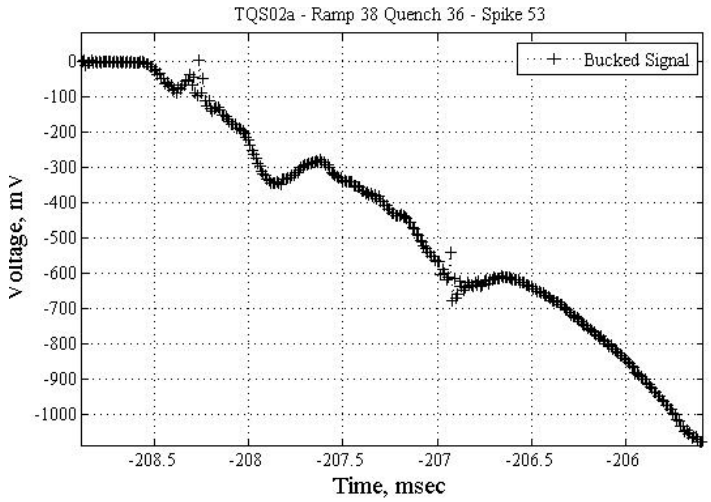

Figure 30: Quench onset of Quench 36 (11770 A)

It is interesting to note that this pattern is similar to the pattern that was seen in quenches 17-20.

This general pattern continued until quench 42, at which point the onset began to show a plateau after about 1 ms. This occurred in quenches 42-52 that began in coil 21 and an example is shown in figure 31 below.

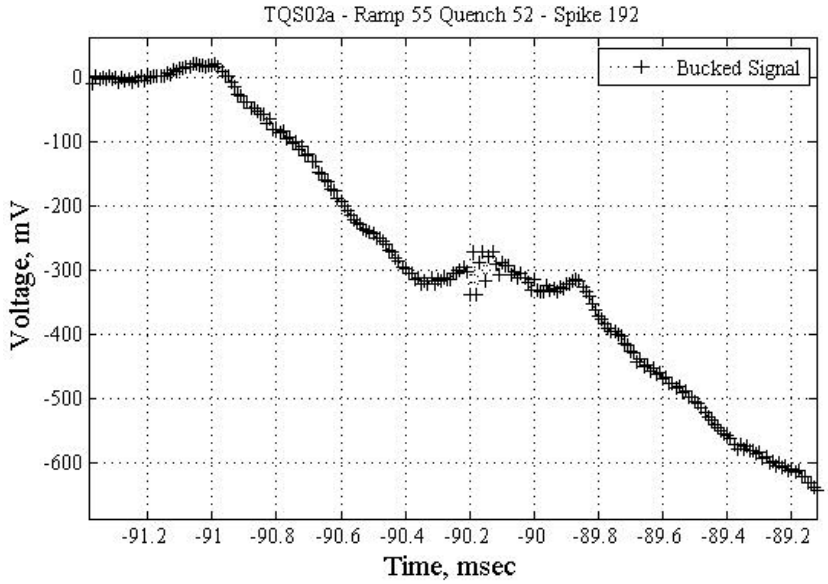

Figure 31: Quench onset of Quench 52 (11925 A)

However, between quenches 42 and 52, there were two quenches that occurred in coil 20, one of which, quench 47, reached the highest current for this magnet, 12.463 kA. These two quenches showed the standard smooth quench onset (Figure 32).

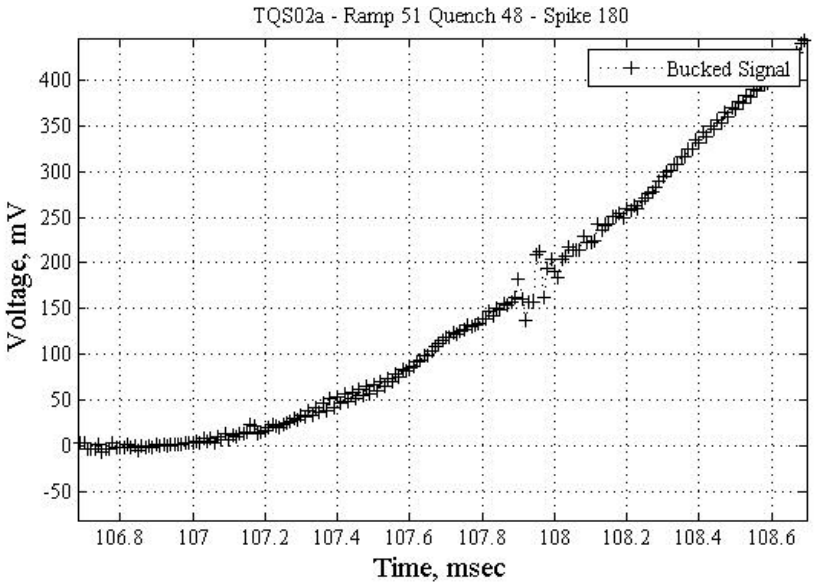

Figure 32: Quench onset of Quench 48 (11957 A)

9. Conclusions

There was a definite correlation between the magnitude of voltage spikes and the current at which they occurred at 4.5 K. The spikes at currents below 5000 A were well defined and generally less than 3 V with only two exceptions. Between 5000 A and 9000 A, the signal become noisier and the spikes less pronounced. Before the noise reduction filter was implemented, above 9000 A, the spikes were less in magnitude than the amplitude of the noise and the VSDS system was most likely tripped by the noise rather than the spike itself.

There was a similar correlation between the magnitude of the voltage spikes and the current at which they occurred at 1.9 K; however, the magnitude of the spikes was roughly an order of magnitude less at this temperature than at 4.5 K. A similar problem was experienced with VSDS threshold being too high to catch the spikes at high current.

Overall, this data is similar in shape, albeit quite different in magnitude, to the data collected for TQC01; the same general shape profile for spike height versus current was seen in both TQC01 and TQS02a.

Once the noise reduction filter was implemented at the VMTF, the clarity of the spikes was much improved. It was also shown that the vast majority of voltage spikes occurred at low currents and had low magnitudes.

The quench onset signals show unusual oscillations in quenches in coil 21 at 20 A/s starting from quench 17. However, no conclusions can be drawn as to the reason of this unusual shape. More examination is needed and will be performed.

References

[1] S. Feher, et al., "Sudden Flux Change Studies in High Field Superconducting Accelerator Magnets", IEEE Trans. Appl. Superconduct., vol 15, no.2 , pp 1591 – 1594.

[2] D. F. Orris et al., "Voltage Spike Detection in High Field Superconducting Accelerator Magnets", IEEE Trans. Appl. Superconduct., vol 15, no.2 , pp 1205 – 1208.

APPENDIX B: TQC01 Voltage Spike Analysis

C. Donnelly, G. Ambrosio, G. Chlachidze

Content

1. Abstract

This note reports the analysis of the data recorded by the VSDS (Voltage Spike Detection System) [1,2] during 63 quenches of the TQC01 superconducting magnet (LARP Technology Quadrapole). Using a MATLAB standalone program, voltage spike profiles (spike magnitude versus current) were generated and it was found that at 4.5 K, most spikes occurred below 3000 A and had magnitudes less than 150 mV. For temperatures below 2 K, the noise levels of the VSDS did not allow for conclusive analysis. It also was found that the magnitude of the voltage spikes increased but the number of spikes decreased with increasing quench sequence at 4.5 K; the opposite effect was observed below 2 K. While examining the onsets of all quenches, normal behavior was found up to quench 28, but irregularities were found intermittently in the remaining quenches.

2. History of TQC01

TQC01 was received on August 1, 2006 and was installed in the VMTF dewar by August 3. The first thermal cycle was completed on August 22, 2006, the second by August 26 and TQC01 was removed from the dewar September 4, 2006.

The magnet was first trained at 20 A/s at 4.5 K, the standard training method. This proved a slow process, as after the 16th quench, the magnet gained roughly 2000 A of quench current, about 75 % of its predicted limit. At this point, it was decided to test the ramp rate dependence at 4.5 K for 6 quenches. Following a thermal cycle, the standard 20 A/s, 4.5 K tests resumed, followed by 20A/s at 1.8 K. The temperature of the magnet was then lowered to 1.9 K and 7 quenches were observed. Another ramp rate study, this time at 1.9 K, was performed; the final 9 quenches of the magnet were observed during a temperature dependence study. Figure 2-1 and Table 2-1 below summarize the test program for TQC01 [3].

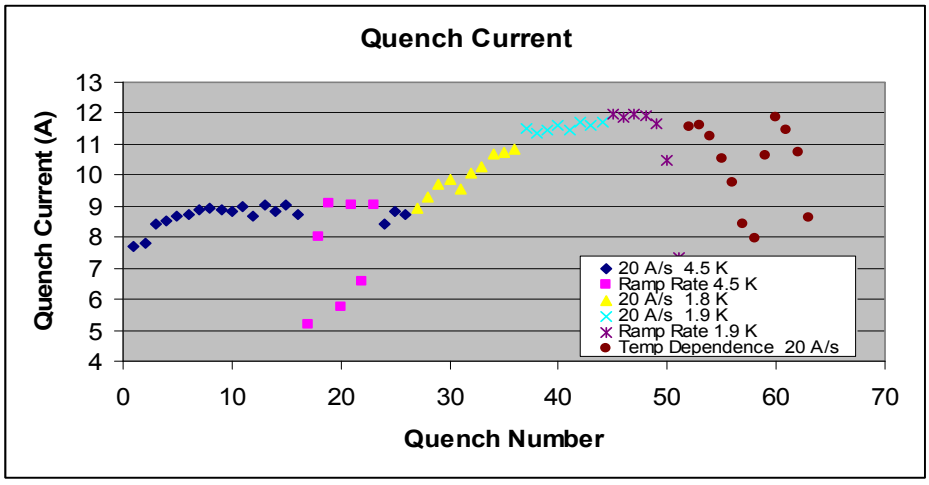

Figure 2-1: Quench History

Table 2-1: Quench History

#	Ramp Rate (A/s)	Temp (K)	Current (A)	Ramp #	Ramp Rate (A/s)	Temp (K)	Current (A)	Ramp #	Ramp Rate (A/s)	Temp (K)	Current (A)
1	20	4.5	7681	**22**	225	4.5	6565	**43**	20	1.9	11623
2	20	4.5	7818	**23**	100	4.5	9065	**44**	20	1.9	11717
3	20	4.5	8446	**24**	20	4.5	8407	**45**	100	1.9	11950
4	20	4.5	8504	**25**	20	4.5	8830	**46**	75	1.9	11862
5	20	4.5	8658	**26**	20	4.5	8757	**47**	125	1.9	11947
6	20	4.5	8756	**27**	20	1.8	8916	**48**	150	1.9	11912
7	20	4.5	8885	**28**	20	1.8	9287	**49**	175	1.9	11680
8	20	4.5	8928	**29**	20	1.8	9693	**50**	200	1.9	10457
9	20	4.5	8877	**30**	20	1.8	9886	**51**	300	1.9	7337
10	20	4.5	8858	**31**	20	1.8	9557	**52**	20	1.9	11541
11	20	4.5	8995	**32**	20	1.8	10093	**53**	20	2.08	11602
12	20	4.5	8671	**33**	20	1.8	10297	**54**	20	2.4	11230
13	20	4.5	9045	**34**	20	1.8	10666	**55**	20	3.24	10514
14	20	4.5	8835	**35**	20	1.8	10743	**56**	20	3.8	9735
15	20	4.5	9060	**36**	20	1.8	10832	**57**	20	4.3	8443
16	20	4.5	8728	**37**	20	1.9	11530	**58**	20	4.45	7953
17	300	4.5	5188	**38**	20	1.9	11361	**59**	20	1.9	10640
18	200	4.5	8030	**39**	20	1.9	11480	**60**	20	1.9	11843
19	150	4.5	9092	**40**	20	1.9	11599	**61**	20	1.9	11461
20	250	4.5	5762	**41**	20	1.9	11468	**62**	20	2.65	10732
21	175	4.5	9037	**42**	20	1.9	11694	**63**	20	4.45	8629

3. Spike Profile Studies

3.1 Standard Training

Quenches 1-16 and 24-26 were observed at standard conditions, 20 A/s at 4.5 K. The spike magnitudes for quenches 2-4, 11, 14-16, and 26 were recorded and are presented in figure 3-1-1 below.

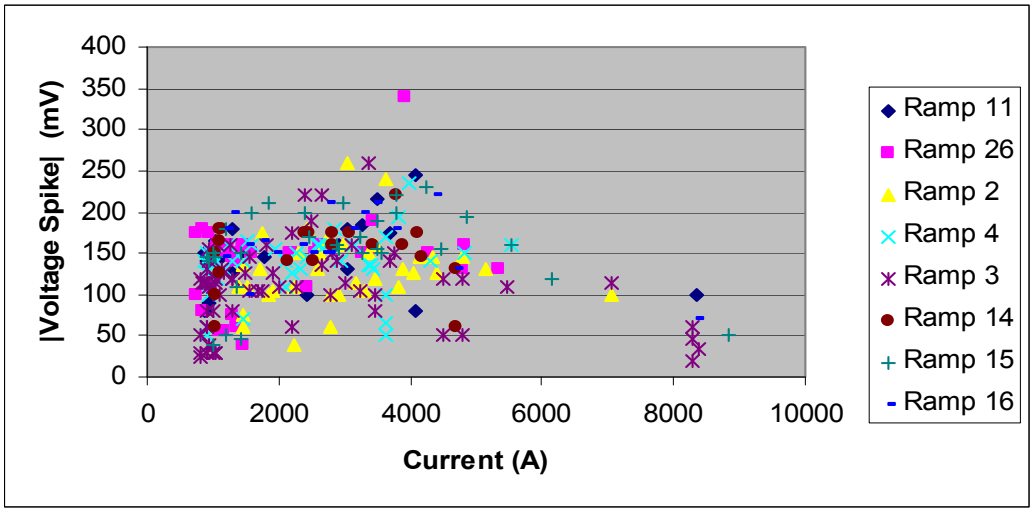

Figure 3-1-1: Standard Training Voltage Spikes

There is a definite pattern to the peak spikes, as there is a smooth rise in voltage spike magnitude followed by a seemingly exponential decay. Isolating the peak voltages shows this trend more clearly (Figure 3-1-2).

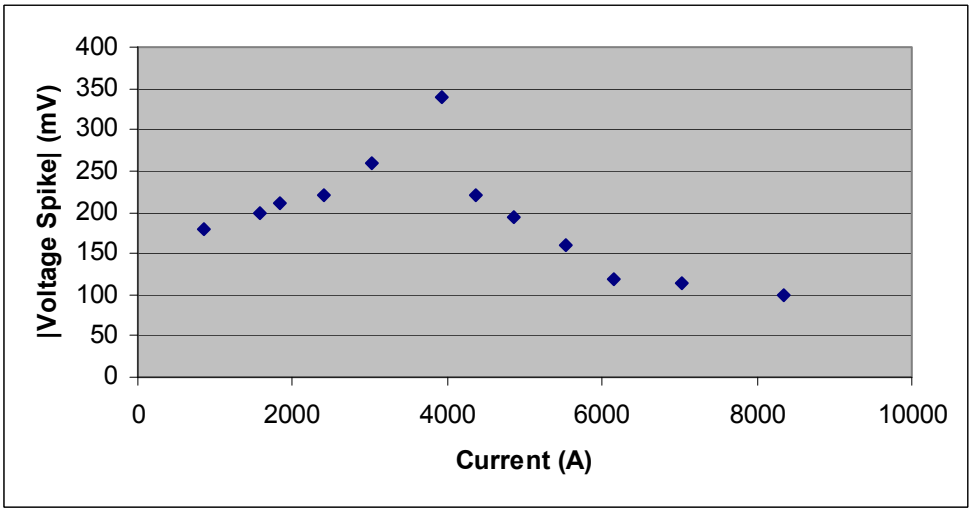

Figure 3-1-2: Standard Training Peak Voltage Spikes

The main purpose of this data collection was to create a profile for the safe operation of a magnet similar to TQC01. The profile produced at this time is a rather messy piecewise function that could potentially be simplified with the edition of more data. The equation of this profile and the profile itself (produced using Maple) are presented below in equation (1) and figure 3-1-3, respectively.

$$f := \begin{cases} 180 & 0 < x \text{ and } x < 1300 \\ 210 & 1300 < x \text{ and } x < 2400 \\ 220 & 2400 < x \text{ and } x < 3300 \\ 260 & 3300 < x \text{ and } x < 3380 \\ 340 & 3380 < x \text{ and } x < 3790 \\ 230 & 3790 < x \text{ and } x < 4850 \\ 195 & 4850 < x \text{ and } x < 5530 \\ 160 & 5530 < x \text{ and } x < 6140 \\ 120 & 6140 < x \text{ and } x < 8350 \\ 100 & 8350 < x \text{ and } x < 10000 \end{cases} \quad (1)$$

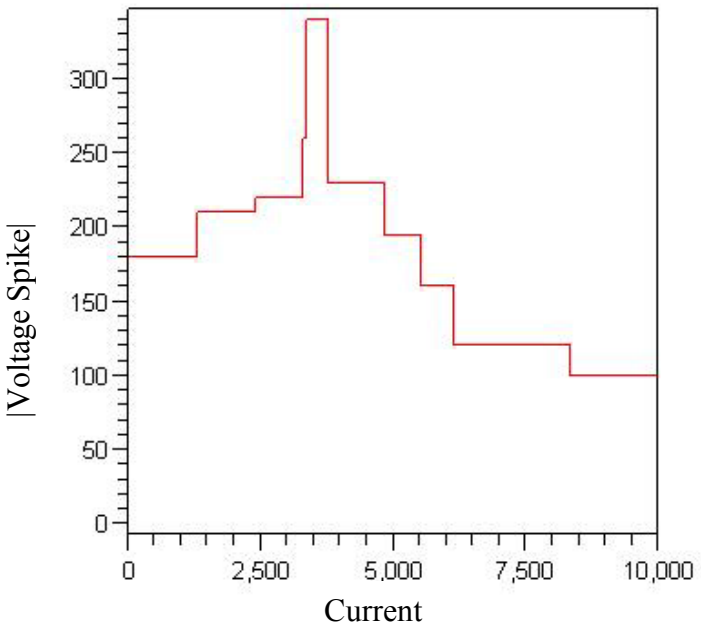

Figure 3-1-3: Profile for Standard Training

This profile creates a dividing line above which no voltage spikes were detected at the current specified. Since none of the spikes used to create this profile induced a quench, the profile could be said to be the upper limit of safe spikes during operation. The profile

itself is indeed complex, but the general trend of initial rise and eventual decrease of spike magnitude is clearly present.

Another interesting investigation proved to be both the number of voltage spikes and the average magnitude of a voltage spike as the standard training progressed. These results are shown in figures 3-1-4 and 3-1-5, respectively.

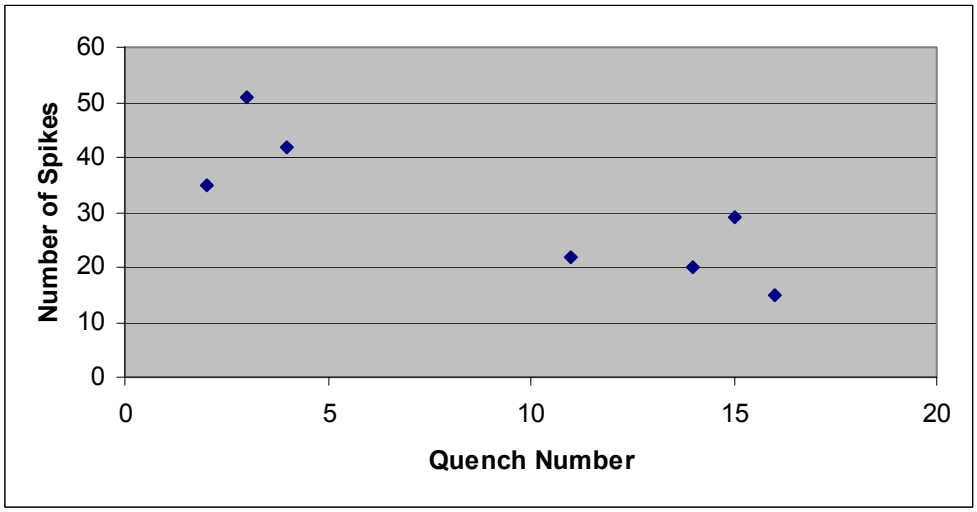

Figure 3-1-4: Number of Spikes versus Quench Number

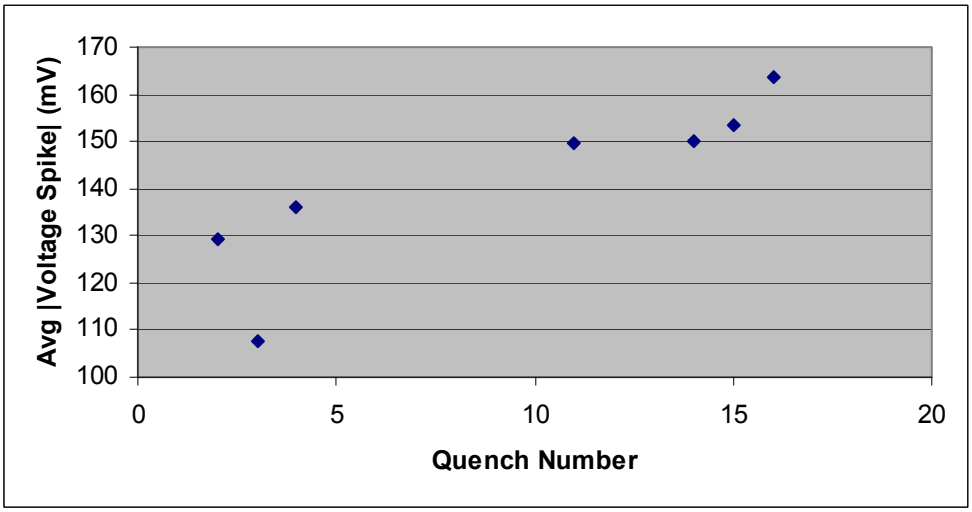

Figure 3-1-5: Average Magnitude of Voltage Spikes versus Quench Number

In standard training, the number of spikes decreased and the average magnitude of the spikes increased with increasing quench number; therefore, repeatedly quenching the magnet could be said to stabilize the magnet in the long run, but short term destabilizations tend to be more pronounced. The reason for the decrease in the number of spikes could lie in Lorentz Forces shifting the wire to more suitable equilibria during a quench sequence; this would serve to stabilize the system and would result in less spikes.

Note that the number of spikes detected is heavily dependent on the VSDS threshold and the noise within the system; a lower threshold with less noise could potentially alter the data in figure 3-1-4.

3.2 Sub 2 K Studies

Quenches 27-44 were sub 2 K studies, divided into 1.8 K for quenches 27-36 and 1.9 K for quenches 37-44. The magnitudes of all the spikes in the 1.8 K ramps and the 1.9 K ramps are shown in figures 3-2-1 and 3-2-2, respectively, below.

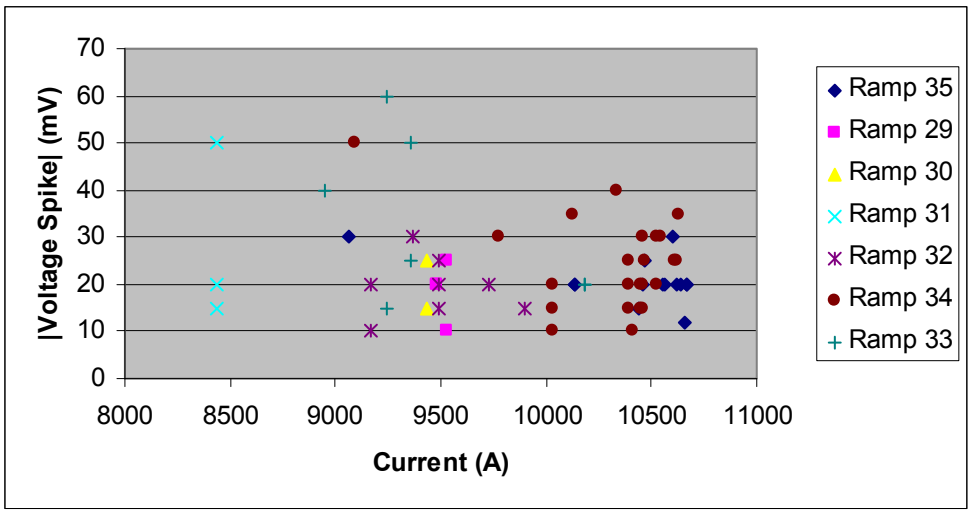

Figure 3-2-1: Magnitude of Voltage Spikes versus Current at 1.8 K

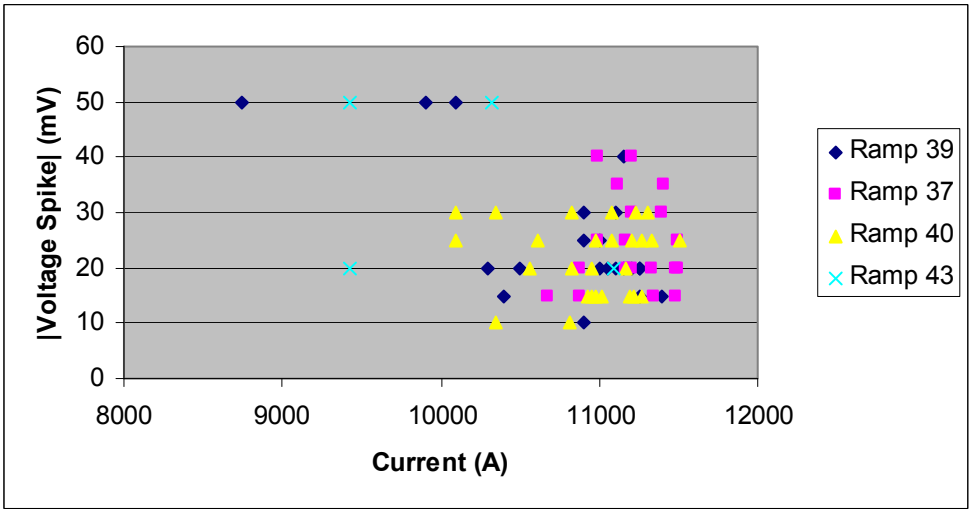

Figure 3-2-2: Magnitude of Voltage Spikes versus Current at 1.9 K

Generally, as current increases, the magnitude of the voltage spike decreases. The profiles for 1.9 K and 1.8 K are given by equations (2) and (3) and are shown in figures 3-2-3 and 3-2-4 below, respectively.

$$g := \begin{cases} 50 & 0 < x \text{ and } x < 10320 \\ 40 & 10320 < x \text{ and } x < 12000 \end{cases} \quad (2)$$

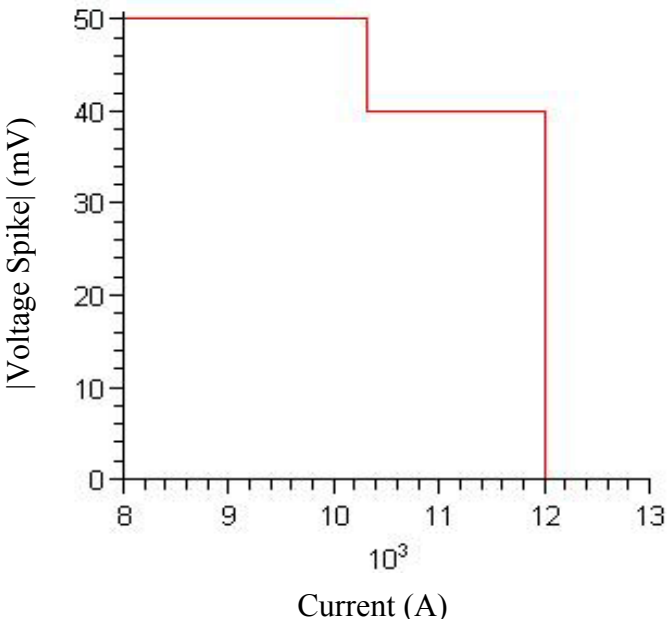

Figure 3-2-3: Profile for 1.9 K

$$h := \begin{cases} 50 & 8000 < x \text{ and } x < 9215 \\ 60 & 9215 < x \text{ and } x < 9265 \\ 30 & 9265 < x \text{ and } x < 10130 \\ 40 & 10130 < x \text{ and } x < 10340 \\ 35 & 10340 < x \text{ and } x < 10630 \end{cases} \quad (3)$$

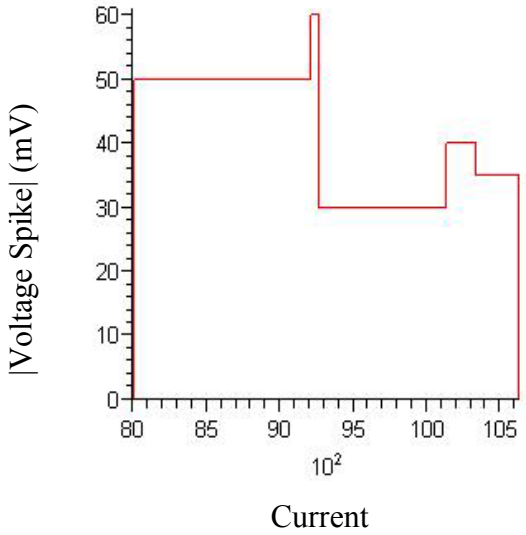

Figure 3-2-4: Profile for 1.8 K

Notice that there were exactly zero spikes detected below 8000 A. This is a result of the VSDS threshold being set too high to detect spikes at these lower currents.

4. Ramp Rate Studies

The dependence of spike magnitude on ramp rate was examined; figures 4-1 and 4-2 below summarize the results at 4.5 K and 1.8 K, respectively.

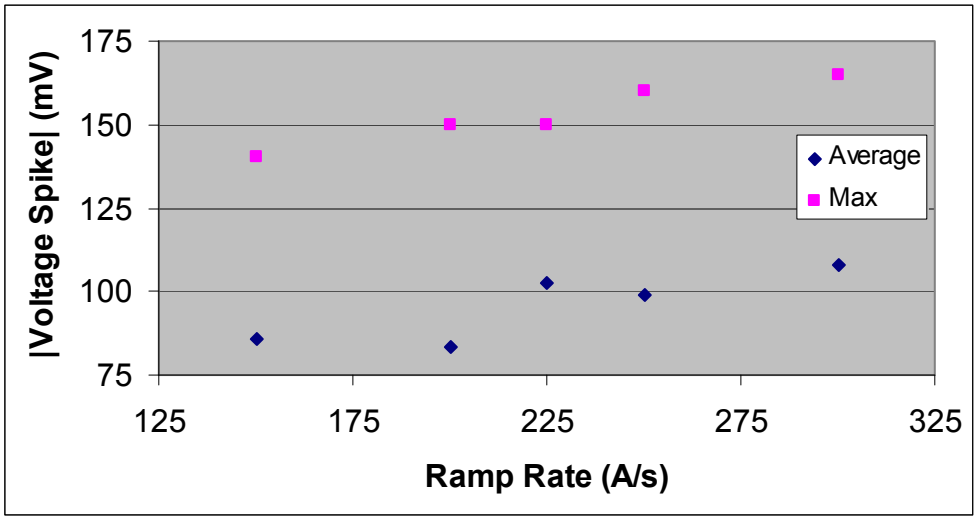

Figure 4-1: Average and Maximum Voltage Spike versus Current at 4.5 K

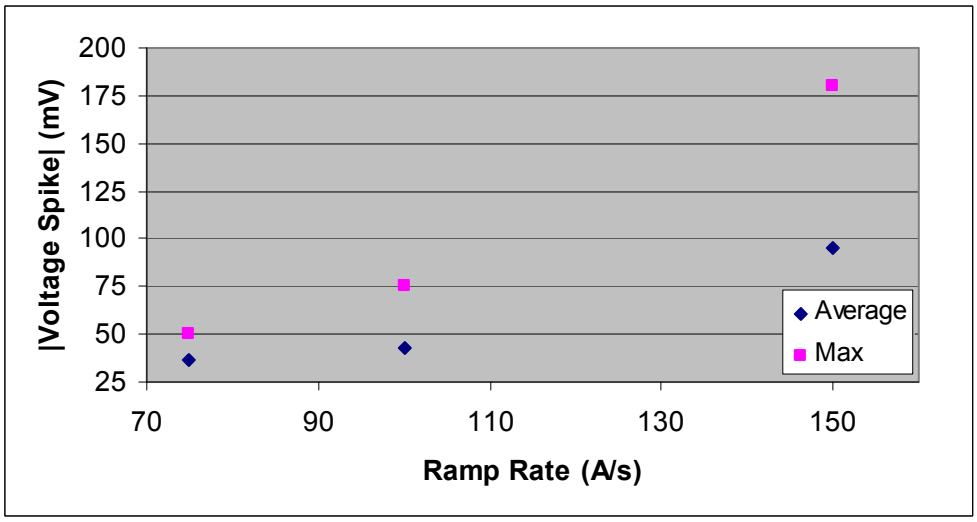

Figure 4-2: Average and Maximum Voltage Spike versus Ramp Rate at 1.8 K

The average and max data point represent the average voltage spike height and the maximum voltage spike magnitude at the various ramp rates. It is important to note that some of the ramp rates did not produce any spikes that were detected by the VSDS; therefore, the only data we have for these ramps is the current and voltage spike for the

quench of the magnet, which is not included in this plot. Also, the ramp rate tended to have a larger impact on the magnitude of the colder magnet.

5. Temperature Dependence Studies

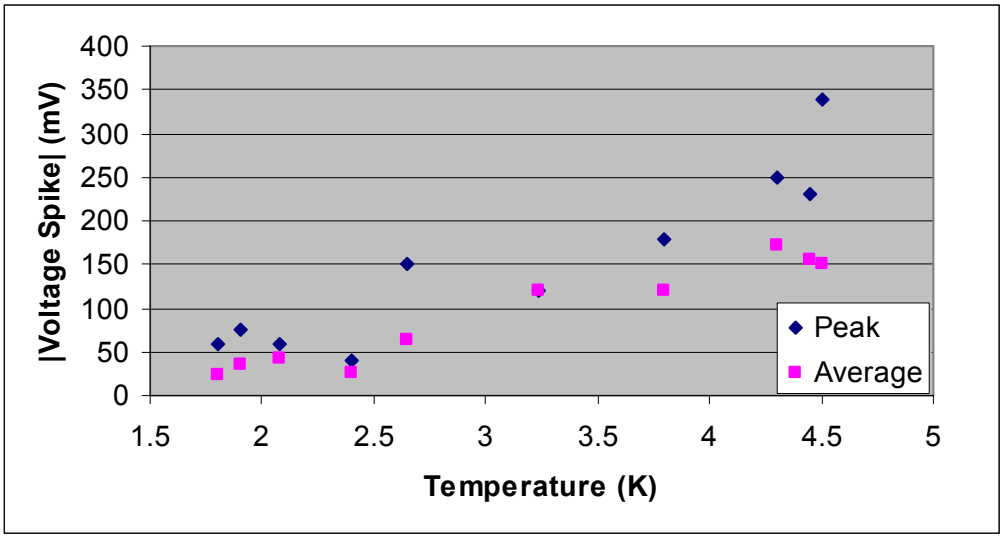

Figure 5-1: Peak and Average Voltage Spike versus Temperature

The data clearly shows that there was an increasing relationship between temperature and voltage spike magnitude where $\frac{d^2V}{dT^2}$ was positive.

6. Quench Onset

The quench onsets of TQC01 showed the standard smooth increase until quench 28 (1.8 K at 20 A/s), at which point, some of the onsets became wavy. Quenches 42-44 (1.9 K at 20 A/s) then showed considerable waviness and occurred in coil 9. Following a ramp rate study and temperature dependence study, three more quenches (59-61) at 1.9 K and 20 A/s were performed. Quenches 60 and 61 occurred in coil 9 and quench 61 showed the considerable waviness that was seen in quenches 42-44. Note that there was not VSDS file for TQC01 quench 60.

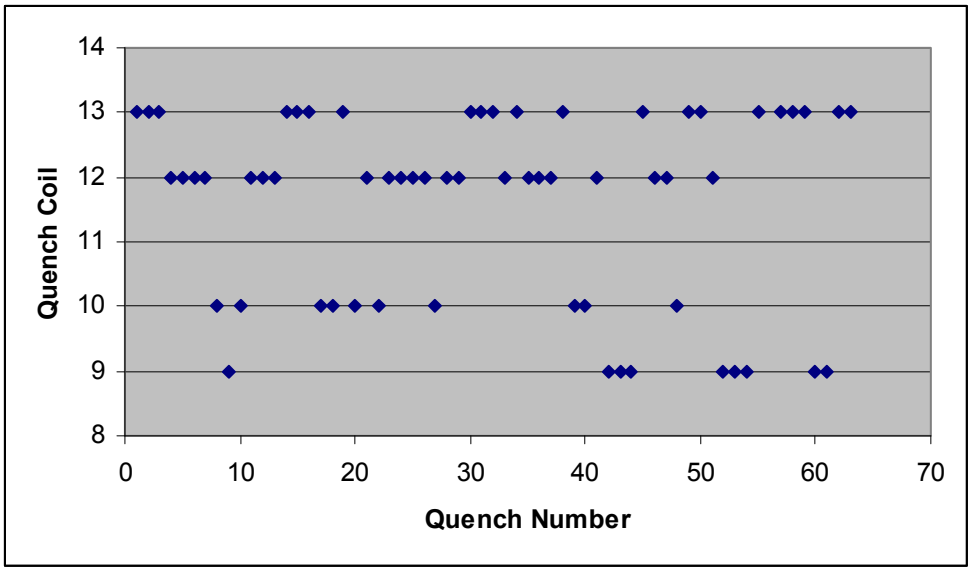

Figure 6-1: Quench Coil versus Quench Number

Most of the quenches showed a standard smooth increase during quench onset, as shown in figure 6-2 below. (Note that the bumps are a result of the power supply.)

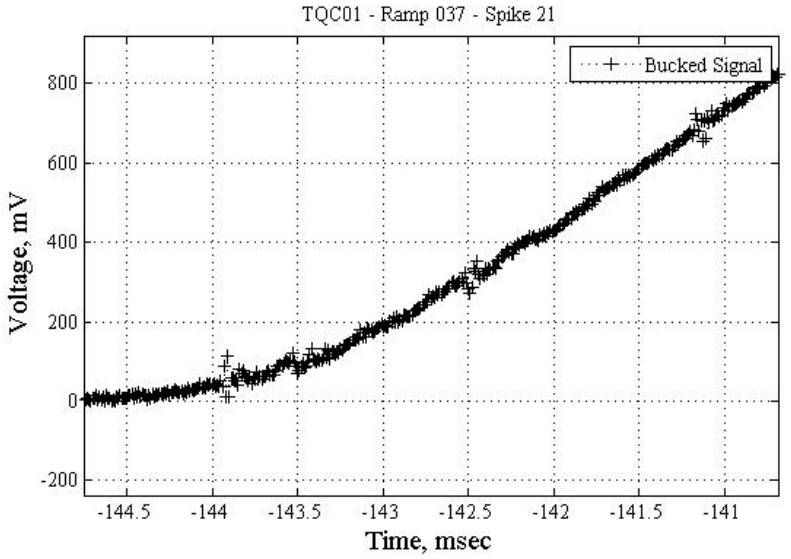

Figure 6-2: Onset of Quench 37

However, as previously mentioned, the quench onset became wavy with some appearance of recovery in some following quenches. This is shown in figures 6-3 and 6-4 below.

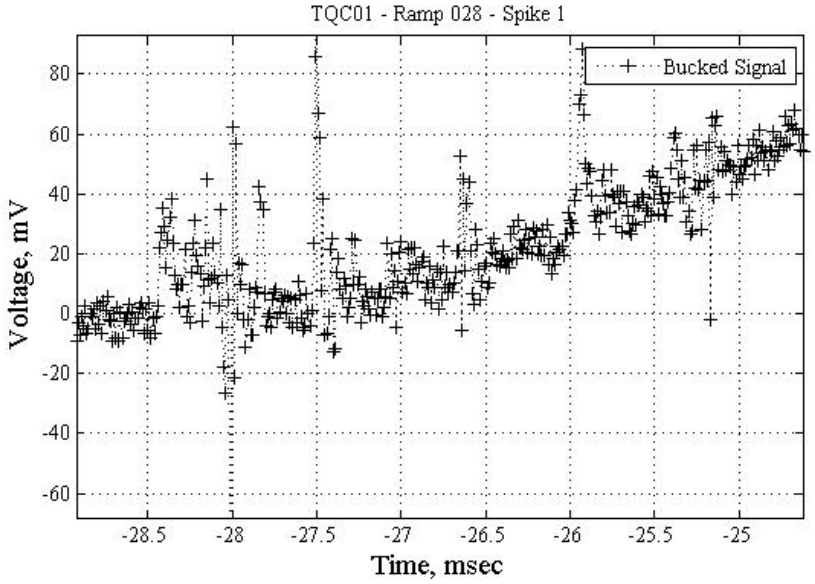

Figure 6-3: Quench Onset of Quench 28

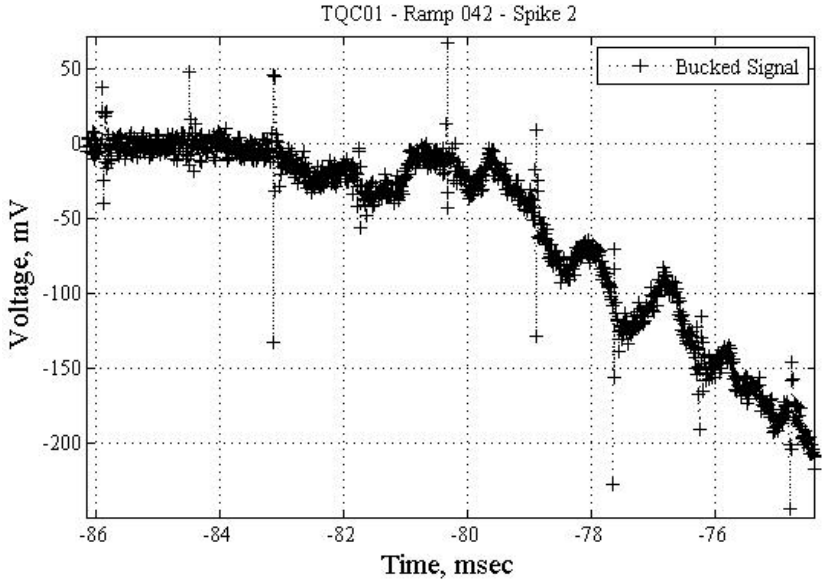

Figure 6-4: Peak and Average Voltage Spike versus Temperature

It is important to note that these aberrations occurred below 2.5 K, which could explain this phenomenon.

7. Statistical Analysis

7.1 Current Distribution

When all the quenches of this magnet are taken as a whole, interesting statistical studies can be performed, namely by creating distributions of where spikes occur with respect to current and spike magnitude. Figure 7-1-1 below is a probability density function, created using MATLAB, of the location of spikes with respect to the current at which they occurred.

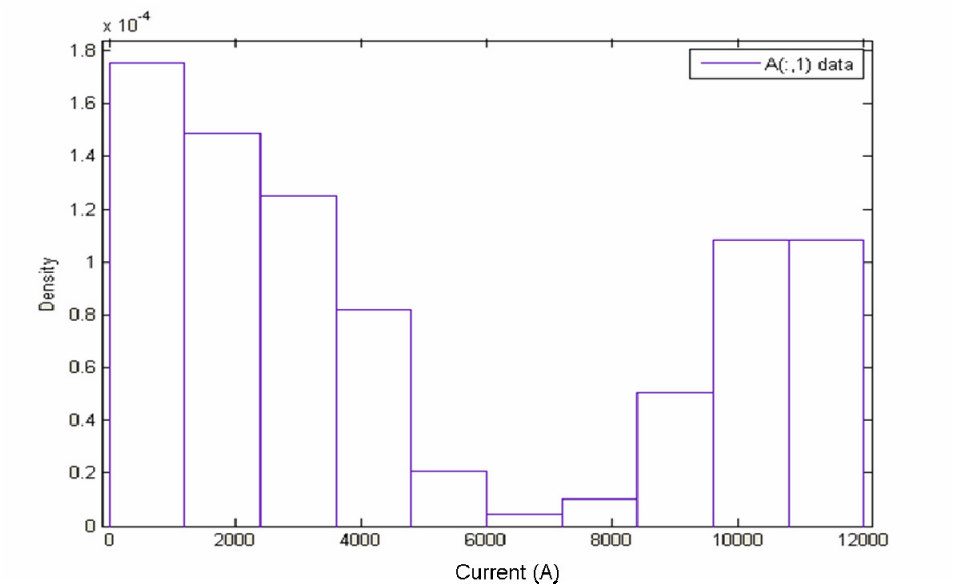

Figure 7-1-1: Current Distribution for TQC01

In this probability density function, the total area under the rectangles is equal to one; therefore, the area each rectangle represents the percentage of the total spikes that occurred at the current bounded by that rectangle. More qualitatively, simply looking at the heights of each of the bars tells the relative (to the other bars) number of spikes that occurred at that range of currents. The peculiarity in figure 7-1-1 lies in the high current regime; normally, one would expect an initial sharp increase followed by a steady exponential decay. The exponential decay is seen in figure 7-1-1 until about 7000 A, at which point the density of spikes begins to increase once again. The reason for this can be seen when grouping data that was taken at 4.5 K and data that was taken below 2 K. Figures 7-1-2 and 7-1-3 show these groups, respectively.

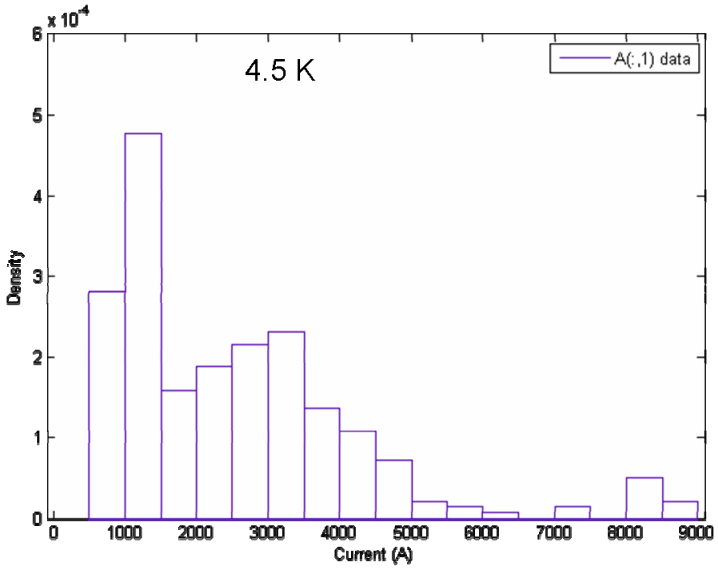

Figure 7-1-2: Current Distribution for TQC01 at 4.5 K

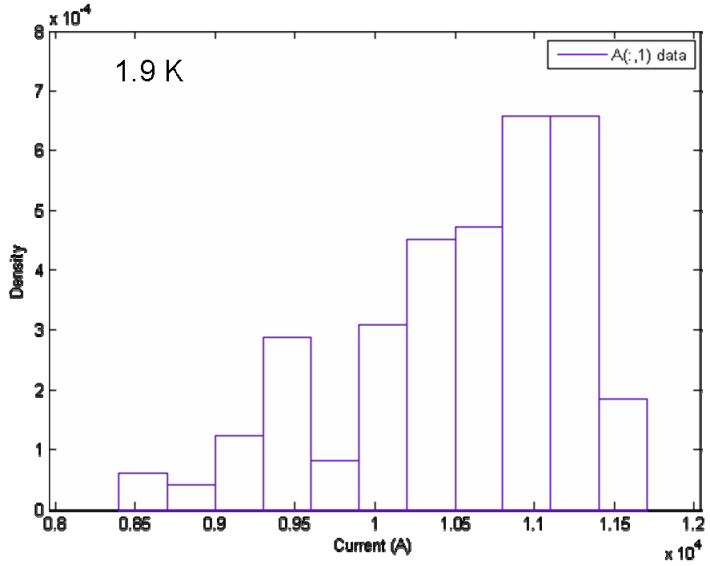

Figure 7-1-3: Current Distribution for TQC01 below 2 K

Figure 7-1-2 has the general steep increase followed by exponential decay that is expected. The dip in density through the 2000 A region can be attributed to the number of data points used to create this plot. The thresholds during these current ramps were generally around 100 mV; however, most of the spikes that occur during a ramp have magnitudes below 100 mV. Therefore, the only way that a spike around 100 mV would be detected was if it was in the same half second window as a spike that did cross the threshold, which inevitably leads to lost spikes. It can be said fairly certainly that if every spike had been captured, the profile would fill out as expected. Because of this, the irregularity in figure 7-1-1 must lie in the distribution created below 2 K, which is shown in figure 7-1-3. The most striking facets of this plot are that there were exactly zero

spikes detected below 8500 A and that as the current increased, so did the density of spikes. This can be attributed once again to the threshold set for the VSDS. It has been shown that spikes below 2 K can be of an order of magnitude less than those seen at 4.5 K [4]. Also, according to the text files that are created with each LabVIEW file by the VSDS, the threshold for these ramps was around 100 mV. Therefore, the VSDS did not detect any spikes below 8.5 kA because the spikes that were expected, few tens of mV, were not large enough to trip the system. The reason the VSDS was tripped at all stems from the noise levels that occur at high currents. Prior to the implementation of a physical noise reduction system on VMTF in July 2007, it was not uncommon to see noise levels above 100 mV at current above roughly 7000 A [4]. Given that TQC01 was tested before this system was installed, it seems clear that these VSDS trips were artificially produced by noise crossing the threshold. The fact that there were many ramps run with this threshold and noise level would lower density of spikes at low currents (since they were not detected) and raise the density at high currents (due to artificial trips). This could be the reason behind the irregularities in the current distribution data.

7.2 Voltage Spike Magnitude Distribution

A similar analysis can be performed on the magnitude of the voltage spikes themselves. Figures 7-2-1 is the probability density distribution for the voltage spike magnitudes for test performed at 4.5 K.

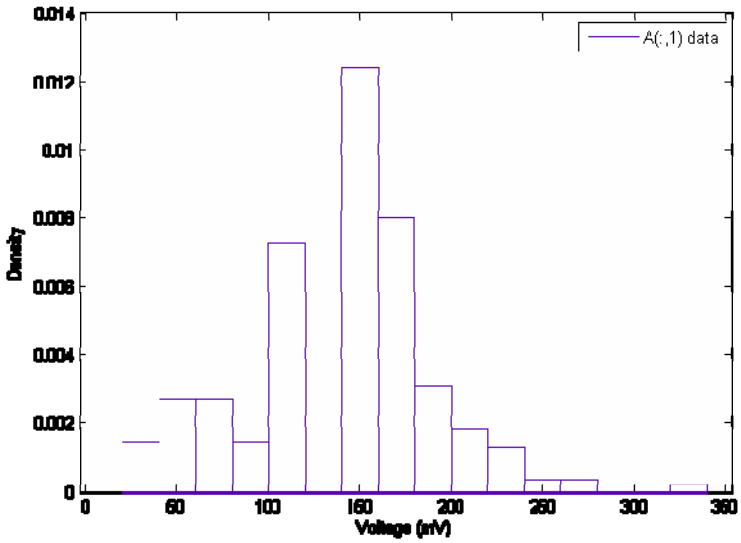

Figure 7-2-1: Voltage Spike Distribution for TQC01 at 4.5 K

This figure is generally what one would expect for a voltage spike distribution. There is an initial increase in the spike height followed immediately by an exponential decay. For this plot, the fact that the initial increase is not perfectly smooth is not a cause for concern as these magnitudes were taken by eye and could vary by +- 5 volts, which could affect the density of spikes within one or more of the bars in the figure. There was one stray

spike of 340 mV during the ramp, which accounts for the little bar in that region. Overall, the data was as expected.

Figure 7-2-2 is a voltage spike magnitude distribution for ramps performed below 2 K.

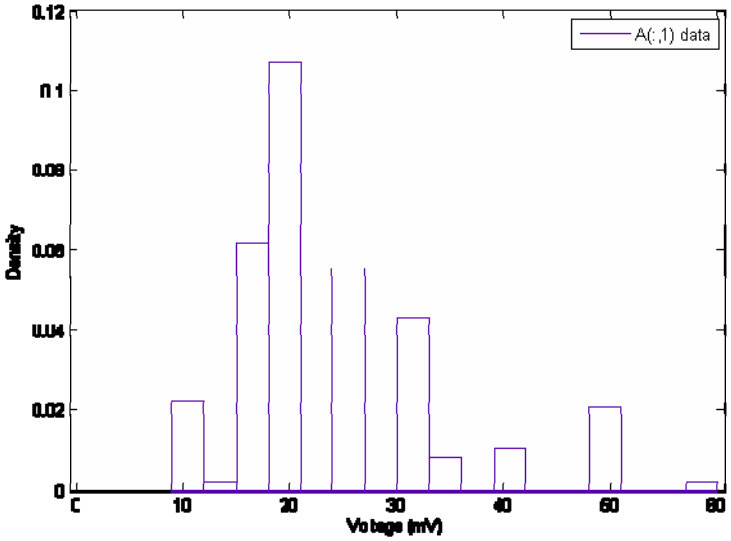

Figure 7-2-2: Voltage Spike Distribution for TQC01 below 2 K

The general form of the data is as expected; however, some clarifications need to be made. When analyzing this data, results were reported to the nearest multiple of 5 mV; therefore, only exact multiples of 5 mV appear on this figure, which explains why some of the expected bars (such as the two missing between 20 and 30) are not present. This does not mean that spikes were not present at these voltages, just that the level of precision of the tool used to perform the analysis did not allow for more accurate reports. With the upgrades to both the data acquisition program and analysis program in the summer of 2007, this should not be a problem in the future.

Figure 7-2-3 is a voltage spike distribution of ramps at all temperatures that were performed at 20 Amps/sec.

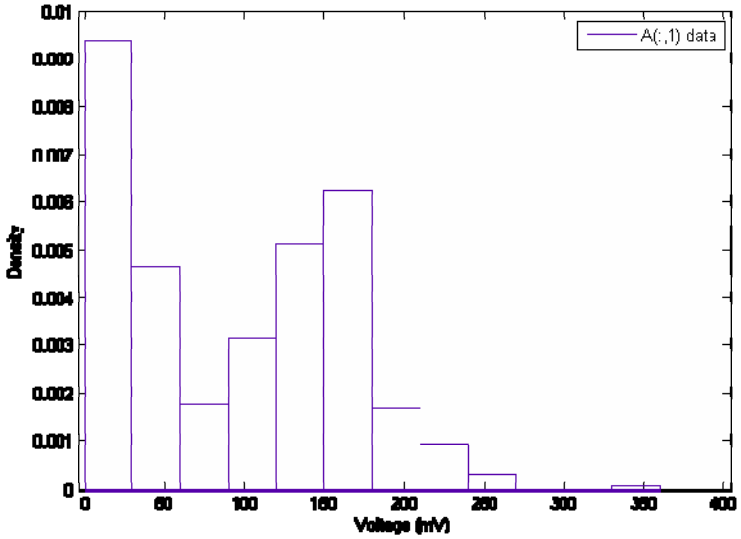

Figure 7-2-3: Combined Voltage Spike Distribution for TQC01

The anomaly with this figure occurs between 50 and 150 mV. One would expect a much smoother decrease in magnitude over this region; instead, a valley can clearly be seen. This figure essentially combines the previous two figures, which exhibited essentially normal behavior, on the same graph. It is speculated that the valley is due to the VSDS threshold being set too high to trip spikes in this region. The spikes at these magnitudes tend to be at low to medium currents, which means that, due to the low noise level at these currents, unless the spikes themselves were high enough the trip the VSDS or they were in the same window as a spike that was large enough, they would not be detected. Moreover, spikes above 150 volts would be able to trip the VSDS themselves and showed normal behavior. Therefore, this problem seems to have arisen from the VSDS threshold being set too high at low current regions, leading to a deficiency of 50-150 mV spikes, and the noise levels tripping the VSDS at high currents, leading to artificial spike detection.

7.3 Combined Distribution

Combining the current and voltage distribution leads to the 3D histogram shown in figure 7-3-1.

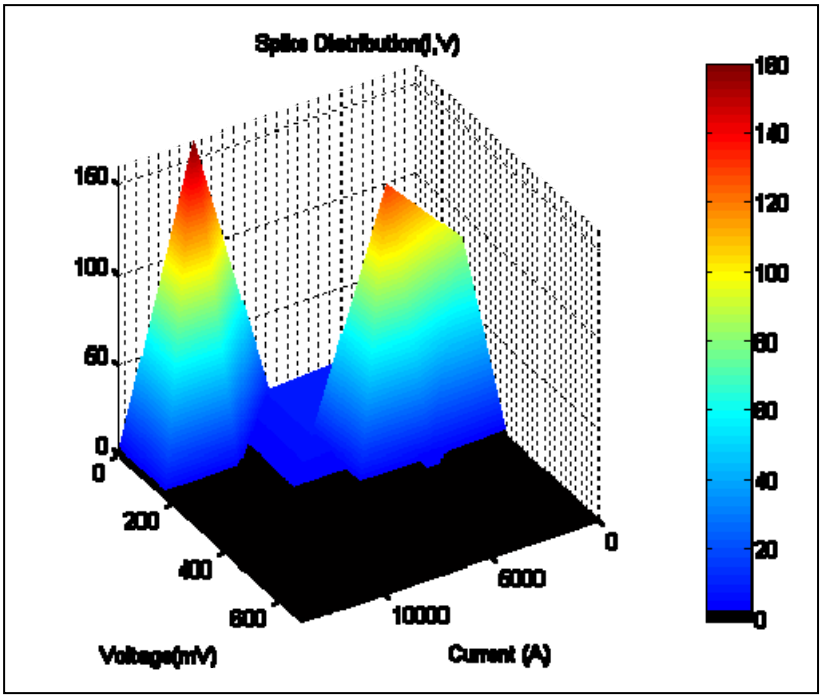

Figure 7-3-1: 3D Density Distribution

This histogram shows the density of spikes at each current and voltage coordinate on the x-y plane; the z axis is normalized to the greatest spike density. The redder the surface the greater the spike density in that area and a black surface indicates a density of zero, i.e. no spikes were present in this area. The lack of smoothness in this plot can be attributed to the same effects that were explained for the individual current and voltage distributions

8. Conclusions

Overall, TQC01 behaved quite well during cryogenic testing. The voltage spike magnitude versus current profile showed the standard increase followed by a steady exponential decay at all temperatures.

The quench onsets of the magnet exhibited a normal steady increase until quench 28, at which point a few irregularities emerged.

Statistical analysis also confirmed, albeit with error from human estimation and noise from the VSDS taken into account, that TQC01 generally behaved as was expected.

References

[1] S. Feher, B. Bordini, et al., "Sudden Flux Change Studies in High Field Superconducting Accelerator Magnets", IEEE Trans. Appl. Superconduct., vol 15, no.2 , pp 1591 – 1594.

[2] D. F. Orris et al., "Voltage Spike Detection in High Field Superconducting Accelerator Magnets", IEEE Trans. Appl. Superconduct., vol 15, no.2 , pp 1205 – 1208.

[3] S. Feher et al., "TQC01 Test Summary", 8-19-06.

[4] C. Donnelly, G. Ambrosio, et al., "TQS02a Voltage Spike Analysis", TD-07-015, 15 July 2007.

Fermilab

APPENDIX C: TQS01c Voltage Spike Analysis

C. Donnelly, G. Ambrosio, G. Chlachidze

Content:

Introduction

TQS01c is a 1 meter long quadrapole magnet built at LBNL and was tested in March 2007. The quench history of TQS01c was presented in TD-07-007 and is summarized in figure 1.

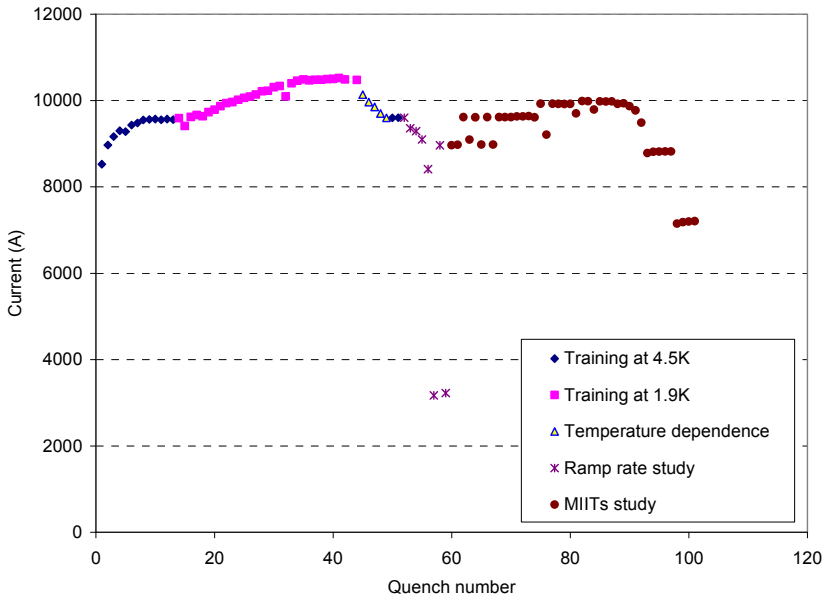

Figure 1: Quench History of TQS01c

The data from these tests were recorded with the VSDS; however, only 31 of the 101 quenches were available at the time of the writing of this report and only the training at 4.5 K and 1.9 K were present within these files. Also, the channel for the current input for the VSDS was improperly installed at the time of testing; therefore; no meaningful current measurements were made. Because of the lack of data from the VSDS for this magnet, it was chosen as a test magnet for the new Automated Voltage Spike Analysis Program, AVSAP; the results generated by the program are presented in this paper.

3. Results

Standard Training

Since there was no current reading for this magnet, we are limited to presenting the voltage spike magnitude and width distributions for the data recorded. The distribution at 4.5 K is presented in figure 2 below.

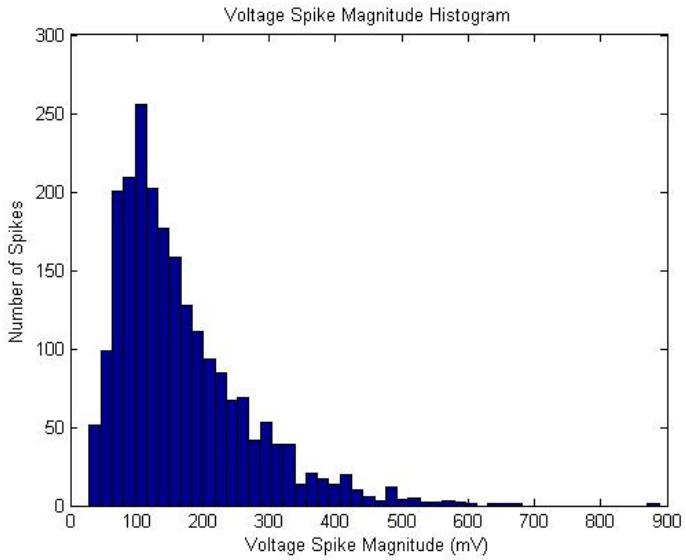

Figure 2: Voltage Distribution at 4.5 K

This figure is a histogram of the number of spikes that occur with the magnitudes given on the x-axis. The y-axis is number of spikes that occurred within the voltage range bounded by the individual rectangles. The initial rise followed by an exponential decay is the expected shape of this profile. Note that the spike with a magnitude of roughly 880 mV was not a failing of the AVSAP, but actually did occur during ramp 14. Figure 3 below is a distribution of the widths that occurred during the ramp tests.

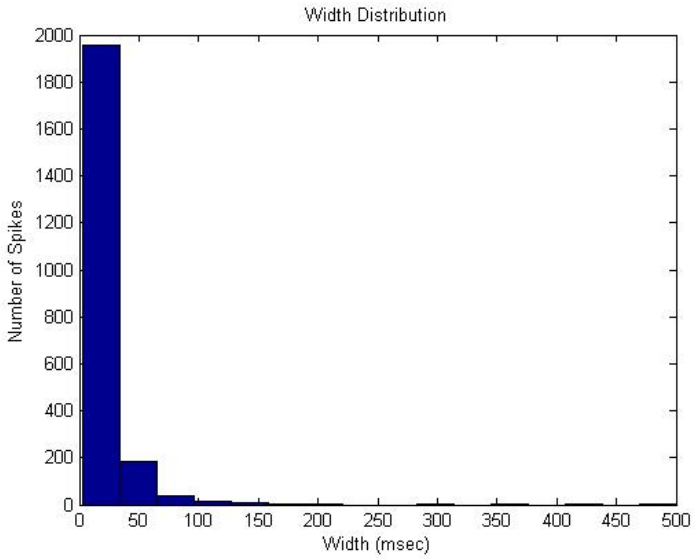

Figure 3: Width Distribution at 4.5 K

From previous manual analysis, it was found that the widths of the spikes during a ramp are generally less than 30 msec, which is confirmed by figure 3. The spikes with widths in the hundreds of msecs are the result of a failure of the program, as the algorithm for

finding widths does not always produce accurate results. However, taken statistically, the distribution of widths generated by the program is realistic.

1.9 K Tests

The voltage spike magnitude distribution for TQS01c at 1.9 K is shown in figure 4 below.

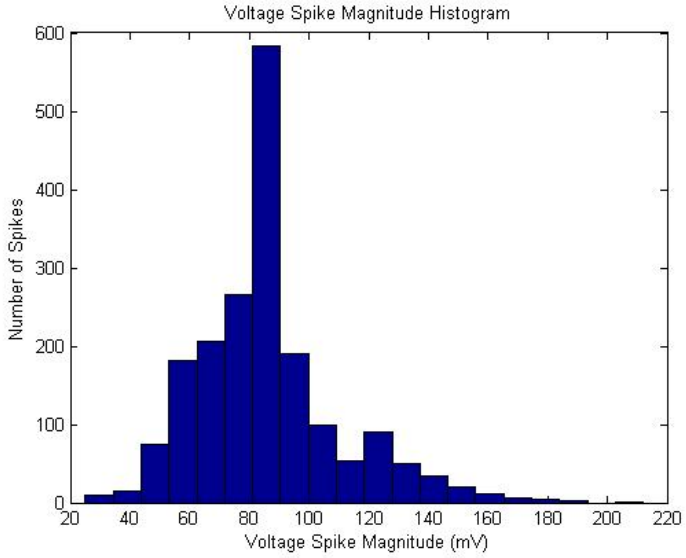

Figure 4: Voltage Spike Magnitude Distribution at 1.9 K

This histogram also shows the characteristic rise and decay expected of voltage spike magnitude. Notice that the peak magnitude is shifted left from figure 2 and that the population to the right of the peak drops off steeply. Moreover, the highest magnitude spike that was detected at 1.9 K was about 210 mV, about a factor of 4 less than the maximum spike at 4.5 K. It is important to note a limitation of AVSAP here, when detecting spikes, the program filters the raw signal, isolates a peak, and then goes back to the original signal to find the magnitude of the peak. This is a good procedure for clean signals; however, if the magnitude of the peak is less than the magnitude of the noise, the program will read the value of the noise as the magnitude of the peak. Given that the magnitude of the noise was between 80 and 100 mV for this ramp, the large peak in number of spikes between 80 and 90 mV could be due to the program reading the value of the noise and not of the peaks at this level. This should not be a problem in the future since a physical noise reduction system was installed on VMTF in the summer of 2007. Figure 5 below shows the width histogram for 1.9 K tests.

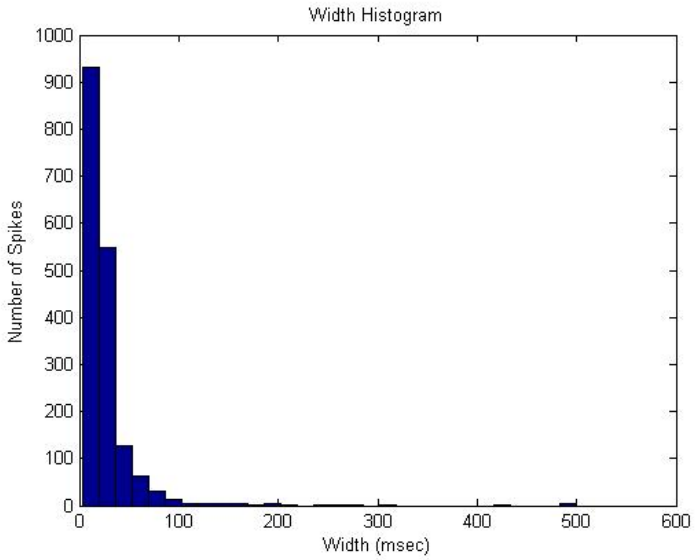

Figure 5: Width Distribution at 1.9 K

Similar to the 4.5 K case, this profile confirms the general observations made by hand during the analysis of previous magnets. Once again, it also shows a limitation of the program in detecting widths, as widths in the hundreds of msec generally do not occur during a ramp.

4. Conclusions

TQS01c performed as expected with regards to width and spike magnitude distributions at all temperatures.

AVSAP performed well on this magnet, with its only limitation being width detection. However, this limitation was known prior to using the AVSAP.

APPENDIX D: SQ02c Quench Onset Analysis

C. Donnelly, G. Ambrosio, G. Chlachidze

Contents

1. Abstract

This note summarizes the results of a quench onset analysis of SQ02c that was performed to better understand the unusual oscillations occurring during the quench onset of TQS02a. SQ02c was chosen because it exhibited degradation during the training process due to high strain in the conductor which could be linked to the irregularities in TQS02a. However, limited correlation between the two profiles was found.

2. Quench Summary

SQ02c was tested in October 2006. The quench history of SQ02c was presented in TD-06-064, LARP-SRD-03, 1/9/07, and is summarized in figure 1 and table I below.

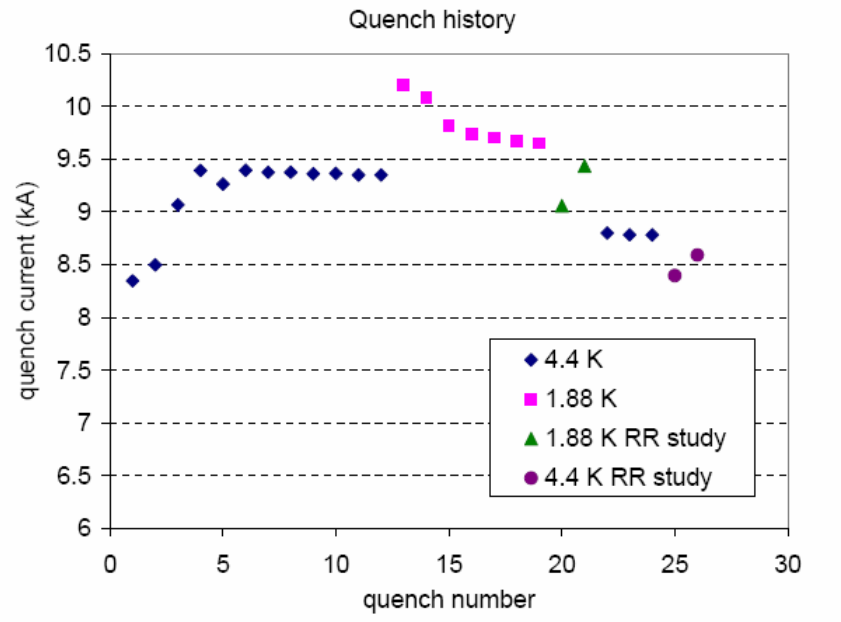

Figure 1: Quench History of SQ02c

Table I: Quench History of SQ02c

File	Quench #	Temp K	Current (kA)	Ramp (A/s)	Time (s)	MIITs	Coil	Quench start	Notes
sq02.Quench.061018192331.224	1	4.4	8.345	20	-0.0045	3.22	17	lead end	
sq02.Quench.061018201624.572	2	4.4	8.497	20	-0.0056	3.41	19	lead end layer jump	
sq02.Quench.061018203639.046	3	4.4	9.067	20	-0.0048	3.58	19	return end outer layer	
sq02.Quench.061018205514.444	4	4.4	9.392	20	-0.0034	3.49	19	return end outer layer	
sq02.Quench.061019114336.661	5	4.4	9.262	20	-0.0034	3.48	20	outer layer pole lead side	
sq02.Quench.061019121017.849	6	4.4	9.394	20	-0.0032	3.46	18	return end	
sq02.Quench.061019133801.124	7	4.4	9.375	20	-0.0035	3.51	18	return end	
sq02.Quench.061019135841.315	8	4.4	9.374	20	-0.0039	3.53	18	return end	
sq02.Quench.061019141603.951	9	4.4	9.361	20	-0.0031	3.47	18	return end	
sq02.Quench.061019143106.621	10	4.4	9.364	20	-0.0027	3.41	18	return end	
sq02.Quench.061019144814.750	11	4.4	9.349	20	-0.0031	3.46	18	return end	
sq02.Quench.061019151430.539	12	4.4	9.349	20	-0.0034	3.49	18	return end	
sq02.Quench.061020123010.322	13	1.89	10.201	20	-0.0027	3.62	19	Inner layer pole turn lead side	
sq02.Quench.061020131003.068	14	1.89	10.081	20	-0.0034	3.73	17	lead end	
sq02.Quench.061020133953.763	15	1.89	9.815	20	-0.0028	3.65	17	lead end	
sq02.Quench.061020143051.158	16	1.88	9.737	20	-0.0029	3.65	17	lead end	waited 25 mins more than in previous quenches
sq02.Quench.061020151230.392	17	1.88	9.703	20	-0.0028	3.63	17	lead end	
sq02.Quench.061020154404.720	18	1.88	9.67	20	-0.0027	3.62	17	lead end	
sq02.Quench.061020165513.595	19	1.89	9.651	20	-0.0032	3.66	17	lead end	
sq02.Quench.061020173621.766	20	1.89	9.058	300	-0.0179	4.66	17	lead end	
sq02.Quench.061020180120.802	21	1.89	9.435	100	-0.0034	3.57	17	lead end	
sq02.Quench.061020195054.448	22	4.4	8.8	20	-0.0034	3.36	17	lead end	
sq02.Quench.061020201530.799	23	4.4	8.783	20	-0.0042	3.42	17	lead end	
sq02.Quench.061020203629.407	24	4.4	8.782	20	-0.0039	3.4	17	lead end	
sq02.Quench.061020204954.375	25	4.4	8.396	300	-0.0039	3.16	17	lead end	
sq02.Quench.061020210255.352	26	4.4	8.592	100	-0.0034	3.25	17	lead end	

3. Quench Onset

The quench onsets of SQ02c followed the standard smooth pattern from quenches 5 to 12, which occurred at 4.5 K and 20 A/s and at 9.262 kA and 9.349 kA, respectively. Also, except for quench 5, which occurred in coil 20, quenches 5-12 occurred in coil 18. Quenches 5 and 12 are shown in figures 2 and 3, respectively. Note that in this figure and in all following figures, the small bumps that are circled come from the power supply.

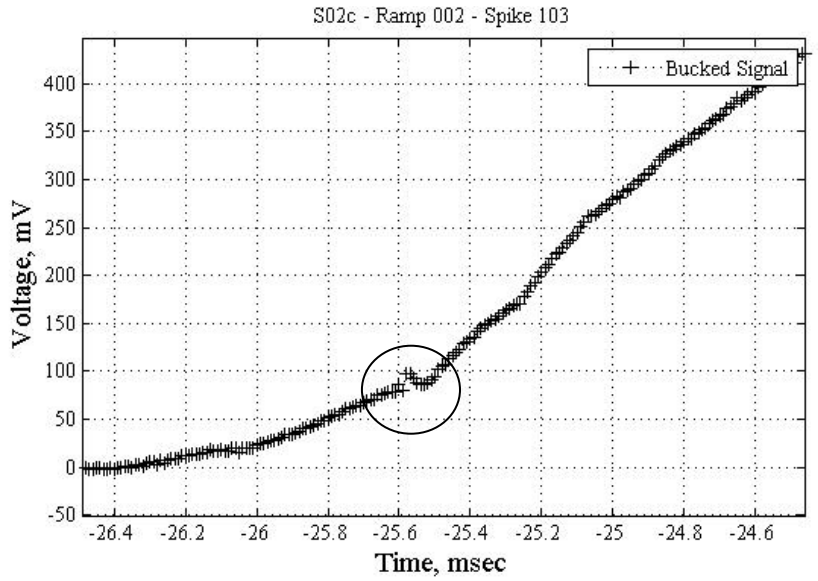

Figure 2: Quench Onset of Quench 5

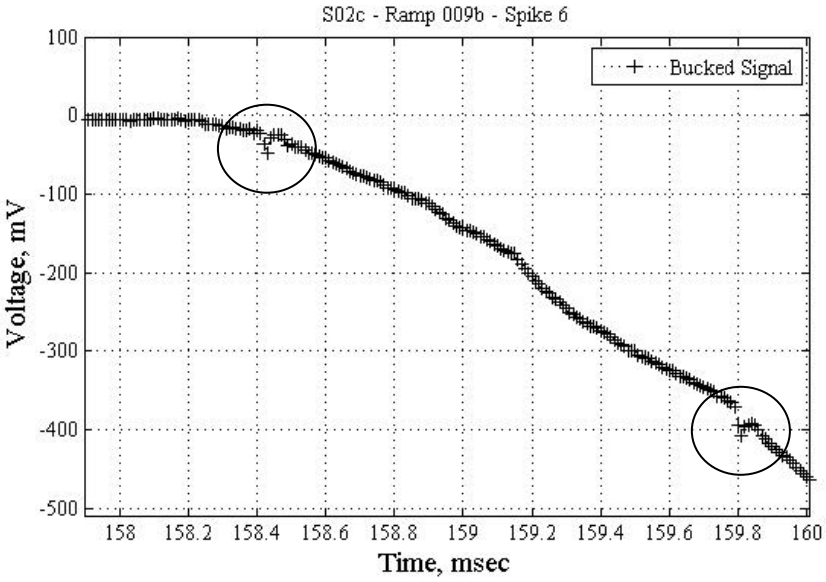

Figure 3: Quench Onset of Quench 12

The next ramp, quench 13, was done at 1.88 K and 20 A/s. Quench 13 reached 10.201 kA and showed an onset with many defined spikes. Moreover, following the spikes, the voltage signal oscillated before settling down. This is shown in figure 4 below.

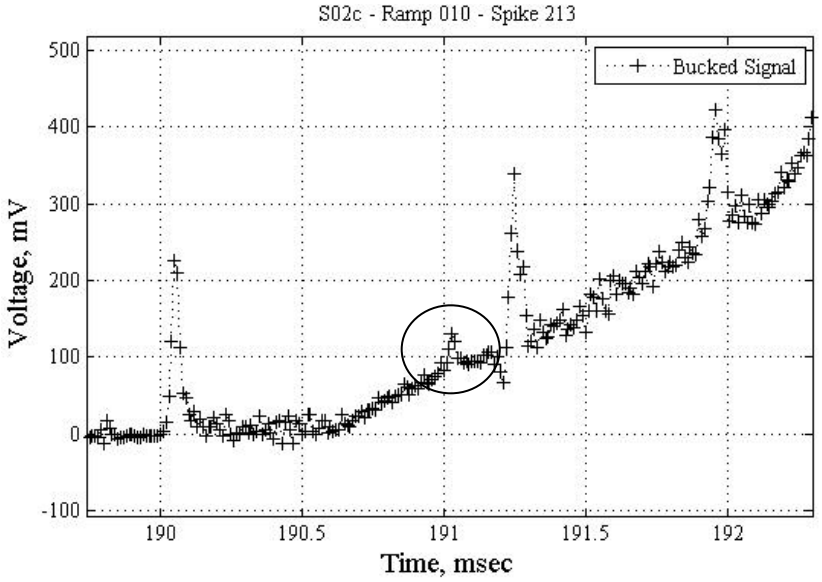

Figure 4: Quench Onset of Quench 13

The remainder of the 1.88 K quenches at 20 A/s (14-19) showed a slightly wavey onset and all occurred in coil 17. Quenches 14 and 19 occurred at 10.081 kA and 9.651 kA, respectively, and are shown below.

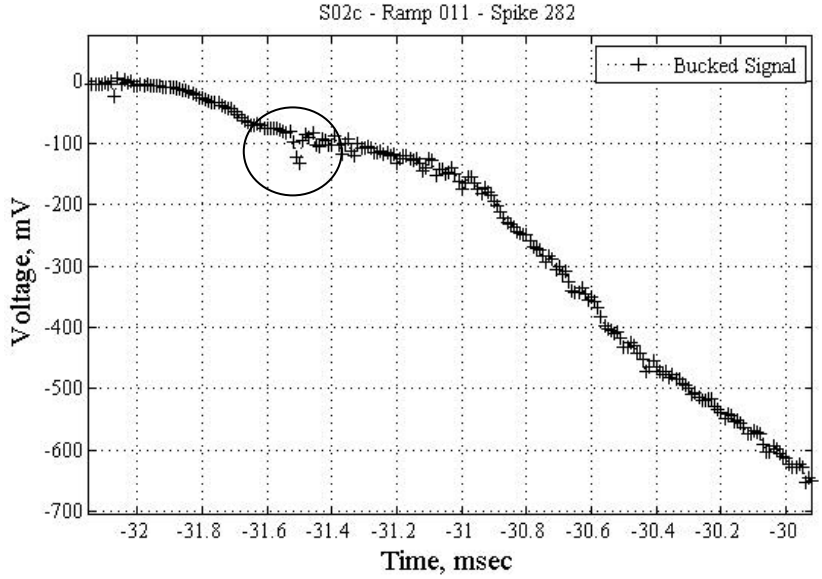

Figure 5: Quench Onset of Quench 14

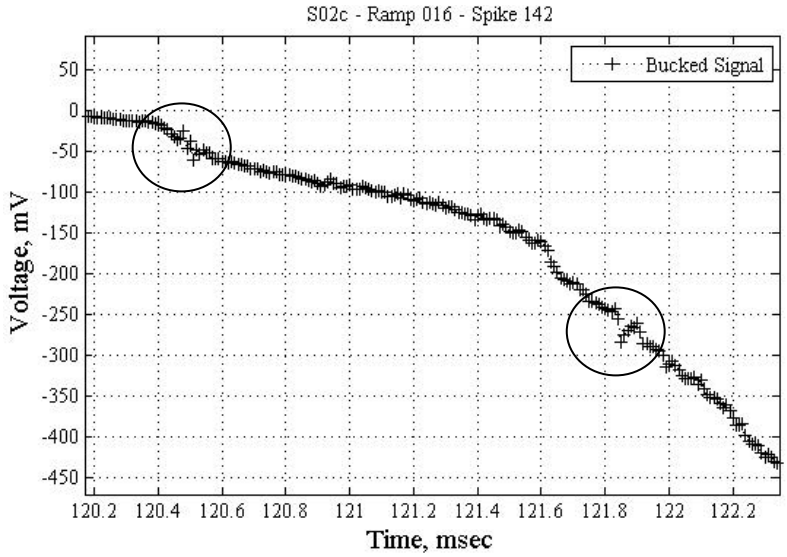

Figure 6: Quench Onset of Quench 19

Following a ramp rate study at 1.88 K, more quenches were performed at 4.5 K and 20 A/s. They followed the same general form as the quenches at 1.88 K, and Quench 22, which occurred at 8.8 kA, is shown as an example in figure 7 below.

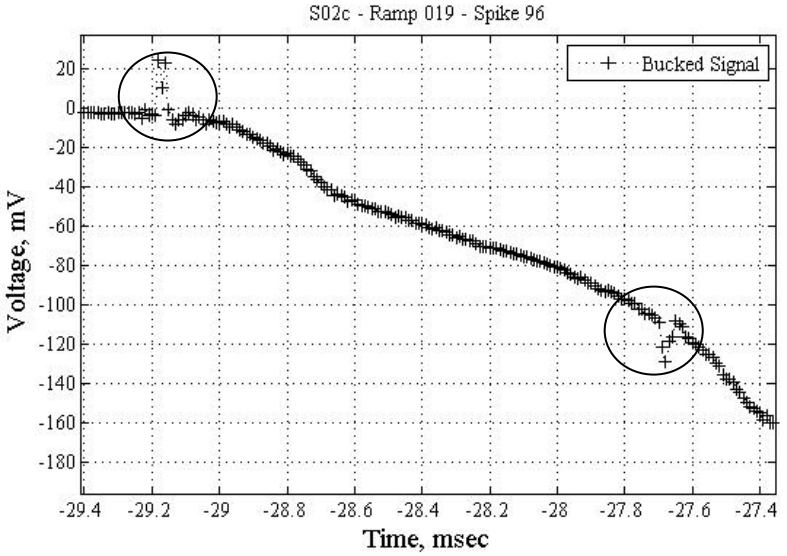

Figure 7: Quench Onset of Quench 22

4. Conclusions

Although SQ02c exhibited wavey behavior during quench onset, it was less pronounced than TQS02a and did not have the change in sign of dV/dt found in the quench onsets of TQS02a. Therefore, a straightforward correlation between the causes of quench onset in TQS02a and SQ02c cannot be established.